Deep-Sea Research Part II 149 (2018) 31–46

Contents lists available at ScienceDirect

Deep-Sea Research Part II

journal homepage: www.elsevier.com/locate/dsr2

On the temporal variability of intermediate and deep waters in the Western Basin of the Bransfield Strait

Eduardo M. Ruiz Barlett[a,*], Gabriela V. Tosonotto[a], Alberto R. Piola[b,c], Marta E. Sierra[a,b], Mauricio M. Mata[d]

[a] Departamento de Oceanografía, Instituto Antártico Argentino, Av. 25 de Mayo 1143 (B1650HMK), General San Martín, Buenos Aires, Argentina
[b] Facultad de Ciencias Exactas y Naturales, Universidad de Buenos Aires (UBA), Intendente Güiraldes 2160 (C1428EGA), Ciudad de Autónoma de Buenos Aires, Argentina
[c] Servicio de Hidrografía Naval and UMI-IFAECI, Av. Montes de Oca 2124 (C1270ABV), Ciudad Autónoma de Buenos Aires, Argentina
[d] Laboratório de Estudos dos Oceanos e Clima, Instituto de Oceanografia, Universidade Federal do Rio Grande (FURG), Rio Grande, RS, 96203-900, Brasil

ARTICLE INFO

Keywords:
Water masses
Western Basin
Bransfield Strait
Modified Circumpolar Deep Water (mCDW)
Warming
Interannual variability
ENSO
SAM

ABSTRACT

The Western Basin (WB) of the Bransfield Strait has a complex water mass structure derived from a variety of sources, and is located next to the Antarctic region most affected by climate change. The WB is one of the three Bransfield Strait deep basins and the one most directly influenced by the waters from the Bellingshausen Sea and Drake Passage. The objective of this paper is to study the variability of the inflow of water masses to the WB and to detect the possible impact of regional climate change. We focus on the modified Circumpolar Deep Water (mCDW) that enters the WB through the northwestern passages. To achieve this goal, this study uses historical hydrographic data collected between 1960 and 2014. Warming ($0.0161 \pm 0.0079\,^{\circ}C\,yr^{-1}$) and lightening ($-0.0023 \pm 0.0010\,kg\,m^{-3}\,yr^{-1}$) of the mCDW core ($\gamma^n$ = 27.85–28.27 $kg\,m^{-3}$) are observed in the WB between 1960 and 2013. The waters within the 27.85–28 $kg\,m^{-3}$ γ^n range presented warming and salinization. Waters deeper than 500 m showed cooling and freshening between the 1960s and 1990s; however, warming and lightening are observed if 1981–2013 is considered. These trends appear to be associated with the positive SAM trend observed since the mid-20th century. Statistically significant negative correlations between θ, S and γ^n of the mCDW core with ENSO were found between 1980 and 2014. During La Niña phases, the mCDW core extended along the southern slope of the South Shetland Islands while during El Niño phases, it was present in patches or was totally absent. Since the 2000s, the mCDW core extends southward within the WB, possibly associated to positive SAM phases. Statistically significant negative correlations between θ and S of the WB deeper waters with ENSO and SAM were found. These waters were in general more saline and denser during negative ENSO and SAM phases. Positive SAM phases with La Niña events suggest the increase (decrease) of mCDW (Weddell Sea shelf waters) contribution to the deep WB during the 2000s. Thus, high interannual variability in the thermohaline properties within the WB seem to be linked to the effect of these modes of climate variability on the source water masses.

1. Introduction

The waters surrounding the Antarctic continent play an important role in global ocean circulation and global climate regulation (e.g., Orsi et al., 1995; Fahrbach et al., 2004). The Bransfield Strait (BS) or Mar de La Flota (Fig. 1) is a relatively deep and narrow (100 km) channel which separates the South Shetland Islands from the Antarctic Peninsula. The BS is filled with water masses derived from different sources having their thermohaline characteristics influenced by local and remote forcing (e.g., Wilson et al., 1999). Also, those waters are an important krill spawning and nursery ground (e.g., Spiridinov, 1996; Atkinson et al., 2004), which plays a key role in the sensible ecosystems of the Northern Antarctic Peninsula. Long-term to interannual changes in hydrographic conditions could have a strong impact on the sensible ecosystem of the WB, from the distribution of krill and salps to changes in penguin populations (e.g., Atkinson et al., 2004; Clarke et al., 2007; Ducklow et al., 2007). The increase in primary production in the Western Antarctic Peninsula (WAP) region since the 1970s could be

* Corresponding author.
E-mail addresses: eruiz@dna.gov.ar, eruizbarlett@yahoo.com.ar (E.M. Ruiz Barlett), gtosonotto@dna.gov.ar (G.V. Tosonotto), piolaar@gmail.com (A.R. Piola), msierra@dna.gov.ar (M.E. Sierra), mauricio.mata@furg.br (M.M. Mata).

https://doi.org/10.1016/j.dsr2.2017.12.010

Available online 20 December 2017

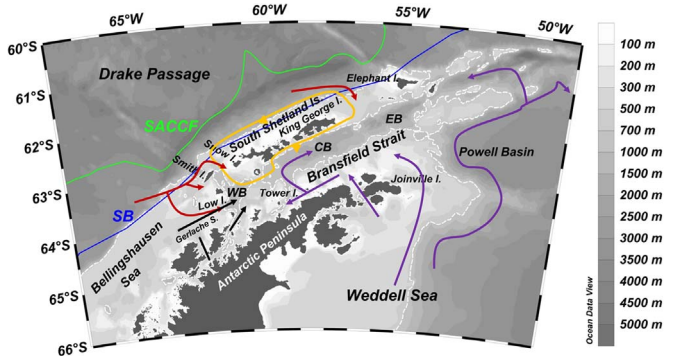

Fig. 1. Schematic pathways of the Circumpolar Deep Water (red arrows), Transitional Bellingshausen Sea Water (black arrows), and Transitional and shelf water of the Weddell Sea (purple arrows) enter into the Bransfield Strait, modified from Dotto et al. (2016) and Sangrà et al. (2017). The schematic circulation in the Bransfield Current System (orange arrows) is adapted from Sangrà et al. (2017). The green and blue lines represent the mean locations of the Southern Antarctic Circumpolar Current Front (SACCF) and the southern boundary of Antarctic Circumpolar Current (SB), respectively (Orsi et al., 1995). The shaded background displays the bottom topography (scale at right) and the thin white line indicates the 700 m isobath. WB = Western Basin, CB = Central Basin and EB = Eastern Basin. (For interpretation of the references to color in this figure legend, the reader is referred to the web version of this article.)

associated with the increase in available light due to the reduction in the sea ice concentration (Montes-Hugo et al., 2009) and shoaling of the nutrient-rich Circumpolar Deep Water (CDW) towards the photic layer (Prézelin et al., 2000, 2004). Therefore, it is important to establish the temporal variability of the BS waters and potential impact on the region.

A portion of relatively cold and saline water from the continental shelf of the western Weddell Sea contours the tip of the Antarctic Peninsula and Joinville Island, enters the BS and flows southwestward along the peninsula, reaching Tower Island (Niiler et al., 1991; von Gyldenfeldt et al., 2002; Zhou et al., 2002; Renner et al., 2012). At that location, the water is mixed with relatively warm water from Bellingshausen Sea and Drake Passage (Niiler et al., 1991). From there, a buoyant gravity current (Sangrà et al., 2017), the Bransfield Current, flows northeastward in a narrow and intense baroclinic jet along the southern South Shetland Islands slope (e.g., Zhou et al., 2002, 2006; Sangrà et al., 2011). Dorsal islands and shallow ridges to the north and west of the BS act as topographic barriers that restrict the flow of intermediate and deep waters from the Bellingshausen Sea and southern Drake Passage. A schematic of this circulation system is shown in Fig. 1.

The waters in the BS can be divided into relatively warm and well stratified waters dominated by characteristics typical of Bellingshausen Sea, and relatively cool, saline and homogeneous transition waters, dominated by characteristics typical of the Weddell Sea (Fig. S1; e.g., Clowes, 1934; Tokarczyk, 1987; García et al., 1994, 2002; Sangrà et al., 2011). García et al. (1994) referred these waters to as Transitional Zonal Waters with Bellingshausen Sea influence (TBW) and Transitional Zonal Waters with Weddell Sea influence (TWW), respectively. The Peninsula Front is a surface structure extending to 100 m depth that separates the shallow TBW from the denser TWW, which occupies the main body of the BS (e.g., Tokarczyk, 1987; García et al., 1994, 2002; Sangrà et al., 2011). On the other hand, the waters close to the surface freezing point (between −1.88 and −1.7 °C) are referred to as Shelf Waters, and are formed by brine rejection during the formation of sea ice in coastal shelves of the southern Weddell Sea and the east coast of the Antarctic Peninsula (e.g., von Gyldenfeldt et al., 2002; Robertson et al., 2002). Following Robertson et al. (2002), these are subdivided into two water masses according to their origin and salinity: High Salinity Shelf Water (HSSW, $S \geq 34.56$) and Low Salinity Shelf Water (LSSW, $S \leq 34.4$).

The CDW is a component of the Antarctic Circumpolar Current (ACC) around the Antarctic continent, and it was subdivided into Upper (UCDW) and Lower (LCDW). Close to the Antarctic continent, northward Ekman leads to upwelling of LCDW (Sievers and Nowlin, 1984; Whitworth et al., 1994; Orsi et al., 1995). Modified CDW (mCDW) is the result of mixing of upwelled CDW with colder and less saline waters from the continental shelf along the southern edge of the ACC (Whitworth et al., 1998). The mCDW enters the BS through the gaps between Smith, Snow and Low Islands (Fig. 1; e.g., Clowes, 1934; Niiler et al., 1991; Wilson et al., 1999; Zhou et al., 2006) and between King George (25 de Mayo) and Elephant Islands (García et al., 1994). The mCDW is characterized by potential temperature within 0–1.5 °C, salinity between 34.5 and 34.72, and low oxygen levels (Fig. S1; Sangrà et al., 2011). Thus, the mCDW is the only source of warm water in the intermediate and deep waters of the BS. MCDW loses heat as it flows onto the WAP shelf, possibly balancing the net heat loss to the atmosphere (Smith and Klinck, 2002; Klinck et al., 2004; Moffat et al., 2009; Couto et al., 2017). In addition, mCDW intrusions represent a high input of nutrients onto the shelf, favoring high biological production (Klinck et al., 2004; Ducklow et al., 2007; Moffat et al., 2009). To date, only few studies analyzed the CDW presence within the BS (e.g., Wilson et al., 1999; García et al., 2002).

BS can be divided into three deep basins that are separated from each other by sills about 1000 m deep. Hereafter the BS basins are referred to as Western, Central and Eastern (Fig. 1). The Western Basin is the warmest of the BS basins (Fig. S1) indicating reduced influence of cold shelf water and greater influence of mCDW as suggested by Gordon and Nowlin (1978). The dense waters in the deep basins are isolated from adjacent waters (Wilson et al., 1999) and therefore preserve signals advected from the northwestern Weddell Sea shelf areas (Azaneu et al., 2013; Dotto et al., 2016; Van Caspel et al., 2017). Shelf waters originate in the Weddell Sea are the major contributor in the bottom waters of the Central (~90% of the contribution) and Eastern (~65%) basins (Wilson et al., 1999), while the remaining percentage is provided by a mixture of CDW and/or Warm Deep Water from the Weddell Sea (Gordon et al., 2000). Thus, in the Central and Eastern basins, intermediate and deep layers are much influenced by cold, fresh signal from the ice shelf melting in the Weddell Sea (e.g., Garcia and Mata, 2005; Dotto et al., 2016; Van Caspel et al., 2017).

Being the BS a semi-enclosed basin where the water mass exchange with surrounding waters is restricted by the bottom topography, it is particularly suitable for the analysis of the temporal variability of water masses (Wilson et al., 1999). Several studies analyzed the hydrographic characteristics of BS waters since the 1920s (e.g., Clowes, 1934; Gordon and Nowlin, 1978; Wilson et al., 1999; Gordon et al., 2000). Studies of temporal variability of deep waters have focused only on the Eastern and Central basins (Gordon and Nowlin, 1978; Wilson et al., 1999; Gordon et al., 2000; Garcia and Mata, 2005; Dotto et al., 2016) or considering the entire BS (Azaneu et al., 2013). The deep waters in the Eastern and Central basins have shown cooling, freshening and lightening since the 1960s caused by the dilution of the shelf waters due to the increase in the fresh water contribution observed in the western Weddell Sea (e.g., Garcia and Mata, 2005; Azaneu et al., 2013; Dotto et al., 2016). Hellmer et al. (2011) observed a dilution (0.09 in 17 years) of shelf waters in the northwestern Weddell Sea between 1989 and 2006. Long-term freshening trends in the Weddell Sea shelf have been reported by Azaneu et al. (2013) and Schmidtko et al. (2014) at rates of $-0.0013\ yr^{-1}$ and $-0.0010\ g\ kg^{-1}\ yr^{-1}$, respectively. These trends may be associated with the freshwater input from the Larsen Ice Shelves ($-37.2\ Gt\ yr^{-1}$ in 2003–2008) to the western continental shelf of the Weddell Sea reported by Rignot et al. (2013).

These changes could also be linked with regional climate change observed since the 1950s. The climate of the WAP has experienced the fastest change observed in the Southern Hemisphere during the last 50 years of the 20th century, with an air warming of 3.7 ± 1.6 °C century^{-1} (e.g., Vaughan et al., 2003). This warming has been associated with a variety of regional changes: upper ocean warming and precipitation increase at the WAP (e.g., Meredith and King, 2005; Uotila

et al., 2007), glacier retreat (Cook et al., 2005; Rignot et al., 2013), southward displacement of sea ice (Morris and Vaughan, 2003), enhanced basal melting of floating glacial ice (Jacobs, 2006; Pritchard et al., 2012), and positive trend of the SAM index since the 1960s (Fig. S2a; Timmerman et al., 2002; Marshall et al., 2006).

Two predominant modes of large-scale climate variability affect the Southern Ocean and in particular, the Antarctic Peninsula region: the Southern Annular Mode (SAM; e.g., Thompson and Wallace, 2000; Marshall et al., 2004) and the El Niño-Southern Oscillation (ENSO; e.g., Yuan, 2004; Loeb et al., 2009). The SAM is an interannual to decadal variability of the difference of zonal mean atmospheric sea level pressure between 40°S and 65°S (Gong and Wang, 1999), which fluctuates between positive and negative phases (Thompson and Wallace, 2000). The increase of the westerly wind pushes the Southern Antarctic Circumpolar Current front (SACCF) and Southern Boundary (SB) (Fig. 1) towards the Antarctic Peninsula during the positive SAM phase (e.g., Marshall et al., 2004; Renner et al., 2012). In addition, at these times, both the Weddell Gyre and the Antarctic Slope Current are accelerated, limiting the connection between the WAP and the Weddell Sea (Renner et al., 2012; Youngs et al., 2015). As consequence, vertical isopycnal shifts at the eastern slope of the Antarctic Peninsula facilitate the export of cold and saline shelf waters in the cross-slope direction and into the deep Weddell Sea (McKee et al., 2011; Kerr et al., 2012). Conversely, during negative SAM conditions, the Weddell Gyre and the current are relaxed due to the decrease of the westerly winds or an increase in the anomalies of the easterly winds. Coastal currents on the eastern Antarctic Peninsula could be intensified, transporting more saline and dense shelf waters originated further south (McKee et al., 2011; Van Caspel et al., 2015) into the BS (Dotto et al., 2016; Van Caspel et al., 2017).

ENSO is characterized by large-scale atmospheric pressure and sea surface temperature fluctuations in the equatorial Pacific (Carleton, 2003) that manifest in high latitudes of the South Hemisphere (Yuan, 2004). During the negative phases of ENSO (La Niña), a low pressure center is located on the WAP, increasing the strength and frequency of northwesterly winds (Yuan, 2004). The location of SACCF and SB displaced southwards, thus moving the warm CDW waters towards the BS (Loeb et al., 2009). Conversely, during the ENSO positive phase (El Niño), northerly winds are less frequent and weaker on the WAP due to the presence of a high pressure center. El Niño phase usually generates warmer temperatures and less sea ice extent in the South Pacific, but generates an opposite response in the South Atlantic sector; while the opposite pattern occurs during La Niña events (e.g., Carleton, 2003; Yuan, 2004). Loeb et al. (2009) found that chlorophyll-a concentrations and primary production are enriched during La Niña, while both decrease during El Niño due to an increase in *Ihlea racovitzai* salps, which are indicative of Weddell Sea waters.

Clem and Fogt (2013) found that the relationships between ENSO and the Antarctic Peninsula climate are significant throughout the western region while relations with the SAM are significant in the northeastern region. Renner et al. (2012) observed that the SAM has a more important role than ENSO in determining the variability of surface currents and the position of fronts around the tip of the Antarctic Peninsula. Therefore, the SAM index can be used here both as a proxy of the wind and to a factor determining the variability of shelf waters that occupy the BS (e.g., Dotto et al., 2016). On the other hand, ENSO can be used to identify the input of warm and saline waters from the Drake Passage into the BS (e.g., Loeb et al., 2009). The suggestion of strong teleconnections between SAM and ENSO (e.g., Stammerjohn et al., 2008; Fogt et al., 2011), and patterns of correlation between the temporal variability of these climate modes and changes in the patterns of distribution of winds, currents, extension and melting of marine and continental ice, and zooplankton species composition and abundance has been reported (e.g., Hall and Visbeck, 2002; Loeb et al., 2009; Renner et al., 2012).

The goal of this paper is to determine the long-term variability of the mCDW inflow within the BS, analyze the intermediate and deep waters in the Western Basin and their possible connection with the climate change. For this purpose, we examined the interannual variability and trends of mCDW core properties within the Western (1960–2013) and Central (1963–2013) basins. Then, the Western Basin water column was separated in layers to search for an explanation of the temporal variability and trends resulting from the connection with the Drake Passage, and Bellingshausen and Weddell seas. Finally, we carried out a combined analysis of regional anomalies of ENSO and SAM together with the spatial variability of mCDW within the BS and the temperature and salinity changes in the Western Basin observed between 1981 and 2014.

2. Data and methods

2.1. Hydrographic data

The available historical CTD and bottle data were obtained from World Ocean Database 2013 (NODC; http://www.nodc.noaa.gov). The Alfred Wegener Institute (AWI) and the Brazilian High Latitude Oceanography Group (GOAL) datasets are available at the PANGAEA repository (http://www.pangaea.de). Temperature, salinity (S) and dissolved oxygen (DO) were selected in the period 1960–2014 between November and March (austral spring/summer) in order to minimize seasonal variability. Only good quality data were used and duplicated hydrographic stations were suppressed. Then, potential temperature (θ) and neutral density (γ^n) were calculated. The instrumental accuracy ranges within data set were 0.001–0.005 °C for θ and 0.003–0.02 for S, respectively (Azaneu et al., 2013; Boyer et al., 2013; Dotto et al., 2016).

The water column in the BS can be divided in three neutral density (γ^n) layers: surface, intermediate and deep waters masses (Jackett and McDougall, 1997). The near-surface waters above ($\gamma^n \leq 27.85\,kg\,m^{-3}$) do not present influence of CDW. The intermediate waters, within $27.85 < \gamma^n \leq 28.27\,kg\,m^{-3}$, are influenced by CDW and mixed with waters derived from the Weddell Sea. Finally, the denser waters ($\gamma^n > 28.27\,kg\,m^{-3}$) are originated in the continental margins of the Antarctic, which include dense shelf waters (e.g., Nicholls et al., 2009). Our analyses focus on the variability of the intermediate and deep waters and, therefore, we only use data collected at locations deeper than 500 m. The data set in the BS was divided based on the depth of each of deep basins in Western Basin, Central Basin and Eastern Basin, and the shallow sills between them (Fig. 2).

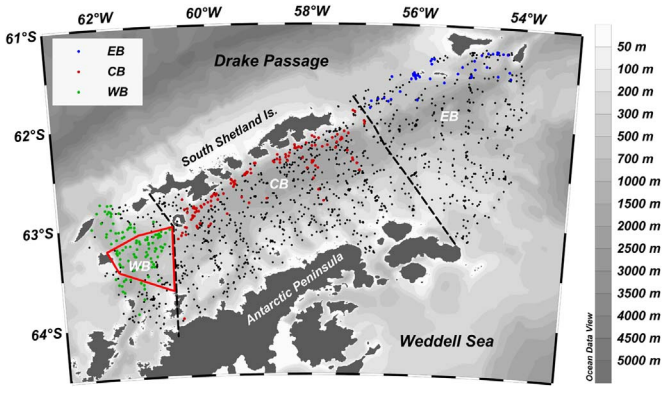

Fig. 2. Location of hydrographic stations available in the Bransfield Strait. Station locations containing modified Circumpolar Deep Water (mCDW) characteristics (see the Section 2.2) are shown in green (WB = Western Basin), red (CB = Central Basin) and blue (EB = Eastern Basin) dots. Dashed lines represent the limits between basins used in this work. The red contour polygon represents the locations of profiles selected for OMP analysis. The shaded background displays the bottom topography (scale at right). (For interpretation of the references to color in this figure legend, the reader is referred to the web version of this article.)

2.2. Modified Circumpolar Deep Water (mCDW) core in the Western and Central basins

The mCDW was defined as waters warmer than 0 °C and saltier than 34.5 (e.g., Sangrà et al., 2011), within the intermediate water neutral density range ($27.85 < \gamma^n \leq 28.27\ kg\ m^{-3}$) and deeper than 150 m. Hydrographic stations containing waters with these characteristics are indicated in Fig. 2. The Eastern Basin was not analyzed because in this study we will focus on the intrusions of mCDW that enter the BS through the northwestern passages (Fig. 1).

To analyze long-term trends in the mCDW core of the Western and Central basins, the maximum potential temperature above 0 °C (θmax ≥ 0 °C) was used. For this analysis, we only considered years when at least two observations of θmax were collected in each basin to estimate more robust trends. The value of θmax was estimated for each profile and grouped in spring/summer for each basin. In addition, depth, S, γ^n and DO at the θmax depth were analyzed. The average and standard deviations around the mean for each year were calculated for the Western (1960–2013) and Central (1963–2013) basins. Linear trends, confidence intervals and statistical p-values (at the 95% confidence levels) were determined.

2.3. Intermediate and deep waters of the Western Basin

To analyze the variability of the intermediate and deep waters of the Western Basin, we separated the water column in two neutral density strata: $27.85 < \gamma^n \leq 28\ kg\ m^{-3}$ and $\gamma^n > 28\ kg\ m^{-3}$ (Note that this includes waters denser that $28.27\ kg\ m^{-3}$). In the less dense layer, we analyzed waters that are approximately in the top 500 m of the water column, which are influenced by mCDW and less influenced by mixing with denser and deeper water masses. Waters deeper than 500 m (approximately $\gamma^n > 28\ kg\ m^{-3}$) were further separated into two deep layers in order to analyze waters less (between 500 and 800 m) or more (deeper than 800 m) influenced by topographic restrictions.

From each profile, we calculated mean values of θ, S, γ^n and DO for the three selected layers. Then, these were grouped into their respective spring/summer, and the average and standard deviations were calculated. Trends were determined in the same way as described in Section 2.2 and calculated until 2013. For the waters deeper than 800 m, we analyzed the period 1981–2013 due to lack of available data in earlier decades. To examine changes in water mass volume, we estimated the depth of 27.85, 28, 28.1 and $28.27\ kg\ m^{-3}$ isopycnals. Also, hydrographic trends were calculated for these isopycnals (except $28.27\ kg\ m^{-3}$ isopycnal). Trends were not calculated for waters denser than $\gamma^n \geq 28.27\ kg\ m^{-3}$ separately due to lack of available data.

We analyzed the hydrographic vertical structure of the Western Basin waters using decadal profiles from 1980s to 2010s (Fig. 3). The profiles represent the average profile for each decade, computing the average in a 10 m window in every 100 m depth layer. We selected this period because the increased number of observations available in the basin. A detailed comparison of all θ, S, γ^n and DO profiles available in the WB from 1960 to 2014 are presented in Fig. S3.

2.4. Modes of climate variability

Monthly averages of the SAM index are available at the State Key Laboratory of Numerical Modelling for Atmospheric Sciences and Geophysical Fluid Dynamics (LASG; http://www.lasg.ac.cn/staff/ljp/data-NAM-SAM-NAO/SAM(AAO).htm). The SAM index can be used as a proxy for the regional wind patterns (Youngs et al., 2015). The monthly Bivariate ENSO Time series (BEST) index (Smith and Sardeshmuk, 2000) obtained from Climate Diagnostics Center (CDC; http://www.cdc.noaa.gov/people/cathy.smith/best/) was used in this work. We selected the BEST index to determine ENSO events because the atmospheric process and the oceanic component, i.e. the Southern Oscillation Index and Niño 3.4 Index, are combined. The normalized and detrended SAM and ENSO time series used in this work are presented in Fig. S2b. Both, ENSO and SAM are smoothed with a 3-month moving average.

The mean spring/summer depth of θmax was positively correlated ($r = 0.86$; $p = 0.01$) with the depth of $\gamma^n = 28\ kg\ m^{-3}$ (not shown). To evaluate the displacement of mCDW within the BS entering from its northwestern end, the 0 °C isotherm on the isopycnal surface of $\gamma^n = 28\ kg\ m^{-3}$ was used as indicator. For this analysis, the years between 1981 and 2014 were selected, taking into account that during this period dense spatial data coverage is available in the BS.

2.5. OMP analysis

The optimum multiparameter analysis (OMP) for the analysis of water masses was first proposed by Tomczak (1981) and further developed by Mackas et al. (1987) and Tomczak and Large (1989). The basic assumption of OMP is that a linear relation exists between hydrographic parameters. The aim of this method is to express all seawater samples as linear combinations of some selected Source Water Types (SWTs). We selected the following water masses to be quantified by OMP: CDW, LSSW and HSSW. SWTs definitions were selected following Dotto et al. (2016) and weights were determined according to Tomczak and Large (1989); both are indicated in Table S1. We selected profiles located in the southern region of the Western Basin (see Fig. 2), where the encounter between mCDW and shelf waters originating in the Weddell Sea occurs. The mean spring/summer contribution to the total mixture in 500–800 m layer and from 800 m to bottom was calculated. The OMP was carried out on the samples collected between 1996 and 2013, since this period includes the required dataset for the analysis, i.e. temperature, salinity and DO. Mass conservation residuals were also calculated as their values are an objective way to check the quality of the OMP solution. Low values indicate that the properties of the samples are well represented by the chosen set of SWTs (e.g., Tomczak and Large, 1989; Poole and Tomczak, 1999; Budillon et al., 2003). In this study, the values obtained for each depth interval were < 7%, which is well within the acceptable threshold (normally, < 10%).

3. Results

3.1. Vertical structure of the water column in the Western Basin (1980s-2010s)

The decadal θ profiles of the Western Basin (WB; Fig. 3**a**) showed substantial differences with depth between 1980s and 2010s. Generally, the highest θ values were found in the 2000s and 2010s and the lowest values were found in the 1990s. Between 400 and 700 m, the θ differences were smaller between the 1980s and 1990s and the warmest values were observed in the 2000s. The decadal S profiles did not show substantial differences with depth (Fig. 3**b**). In the 100–300 m layer, lower S values were found in the 1990s and 2000s. Deeper than 300 m, the S differences between decades were smaller and generally were not significant. In general, the saltiest deep waters (deeper than 1000 m) of the study period were observed in the 2000s. The 2000s γ^n profile (Fig. 3**c**) showed lower values compared with the rest of the analyzed decades. Below 800 m, the γ^n differences in the 1980s and 1990s were higher and generally significant compared with the rest of the analyzed decades. The isopycnal of $28.27\ kg\ m^{-3}$ deepened over time from ~850 m during 1980s to ~1100 m during the 1990s. Waters denser than $28.27\ kg\ m^{-3}$ were not found after the 1990s in the WB.

Fewer DO data were available compared with the other parameters (Fig. S3). The decadal DO profiles (Fig. 3**d**) presented substantial differences with depth. Between the 1980s and 2000s, the DO content showed a decrease between 100 and 300 m (reaching differences of $\sim 0.5\ mL\ L^{-1}\ decade^{-1}$). In deeper waters, the lowest DO values of the

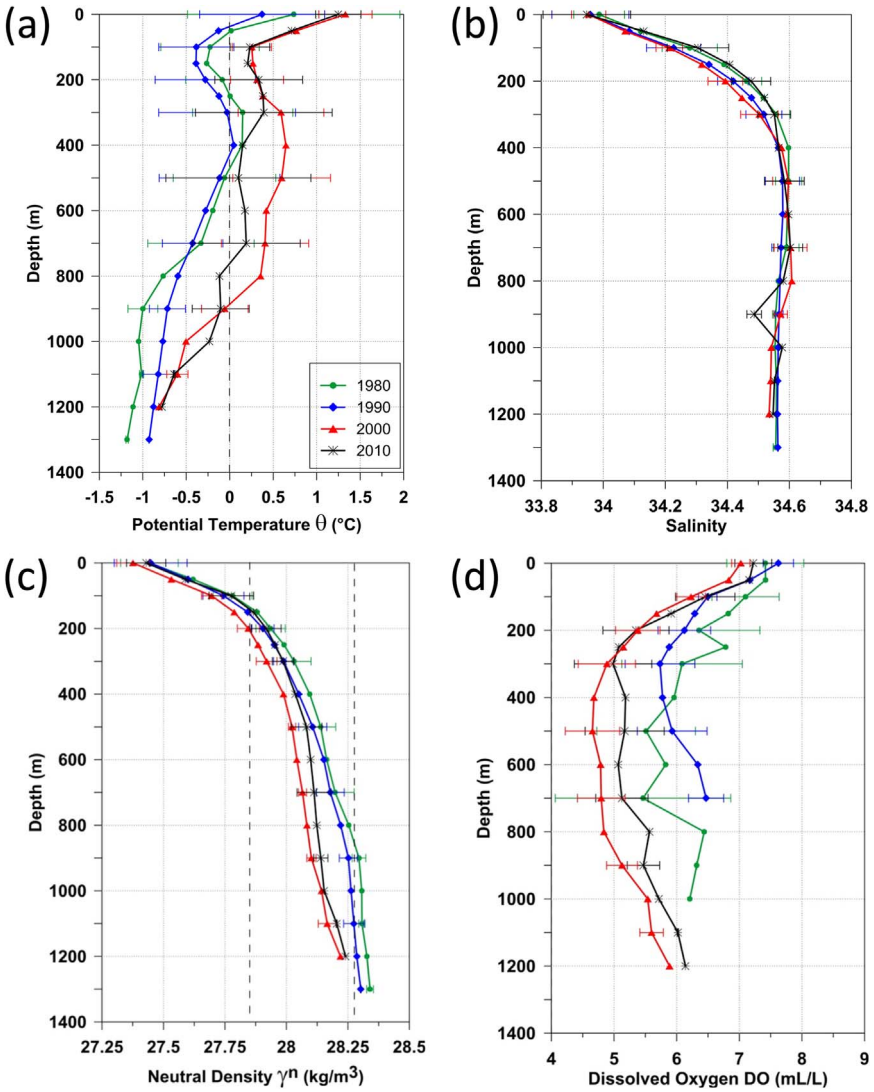

Fig. 3. Decadal profiles of (a) potential temperature (θ), (b) salinity (S), (c) neutral density anomaly (γ^n) and (d) dissolved oxygen (DO) for stations deeper than 500 m in the Western Basin (1981–2014). Decade colors references are included in panel (a). Horizontal bars represent one standard deviation around to certain chosen depth. Vertical dashed lines represent 0 °C, 27.85 and 28.27 kg m^{-3}.

study period were observed in the 2000s whereas the highest DO values were observed in the 1990s (although these profiles did not reach the deep depths of the basin).

3.2. Long-term trends

3.2.1. Maximum potential temperature in the mCDW within the Western (1960–2013) and Central (1963–2013) basins

The temporal evolution of the mean spring/summer θmax as well as depth, S, γ^n and DO for θmax are shown for the Western (1960–2013; Fig. 4**a–e**) and Central (1963–2013; Figs. S4a-S4e) basins, respectively. The estimated trends and their statistically significance are summarized in Table 1. In the WB, an increase of θmax and a decrease of γ^n of θmax were observed between 1960 and 2013 (Fig. 4**a**, **d** and Table 1). On the other hand, in the Central Basin between 1963 and 2013, decreasing values of S and γ^n of θmax were recorded (Figs. S4c, S4d and Table 1).

3.2.2. Intermediate and deep waters in the Western Basin

To identify trends in the hydrographic properties of the WB layers described in Section 2.3, we consider the full period (1960–2013). All of the trends and their statistically significance are summarized in Table 2. Between 1960 and 2013, the 27.85 < γ^n ≤ 28 kg m^{-3} layer presented increased θ and S trends (Fig. 5**a** and **b**). Fewer DO data were available in comparison with the other parameters; however, the results showed a statistically significant decrease between 1981 and 2013 (Fig. 5**d**). The θ and S values showed an almost monotonic increase from 1999 to 2011 and decrease from 2011 to 2014 (Fig. 5**a** and **b**).

For the 500–800 m layer, the hydrographic property trends were not significant during the full period (not shown). However, between 1960 and 1999, the decreasing values of θ and S were statistically significant (Fig. 6**a-b** and Table 2). That period was characterized by cooling of the 500–800 m layer associated with Weddell Sea shelf water dilution. The drastic change in the hydrographic parameters observed in the region during the 2000s (see Section 3.3) seems to have influenced the trends obtained for the full period. Increasing θ and decreasing γ^n were recorded between 1981 and 2013 (Fig. 6**a** and **c**). For the layer deeper than 800 m, trends during 1981–2013 (warming and lightening; Fig. 7**a, c** and Table 2) were consistent with those observed in the 500–800 m layer in the same period.

Finally, the depth of the 27.85, 28 and 28.1 kg m^{-3} isopycnals showed significant deepening between 1981 and 2013 (Fig. 8**a** and Table 2). The 27.85 and 28 kg m^{-3} isopycnals presented warming (Fig. 8**b**) whereas only the 28 kg m^{-3} isopycnal showed a significant increase in S (Fig. 8**c**) and decrease in DO content (Fig. 8**d**).

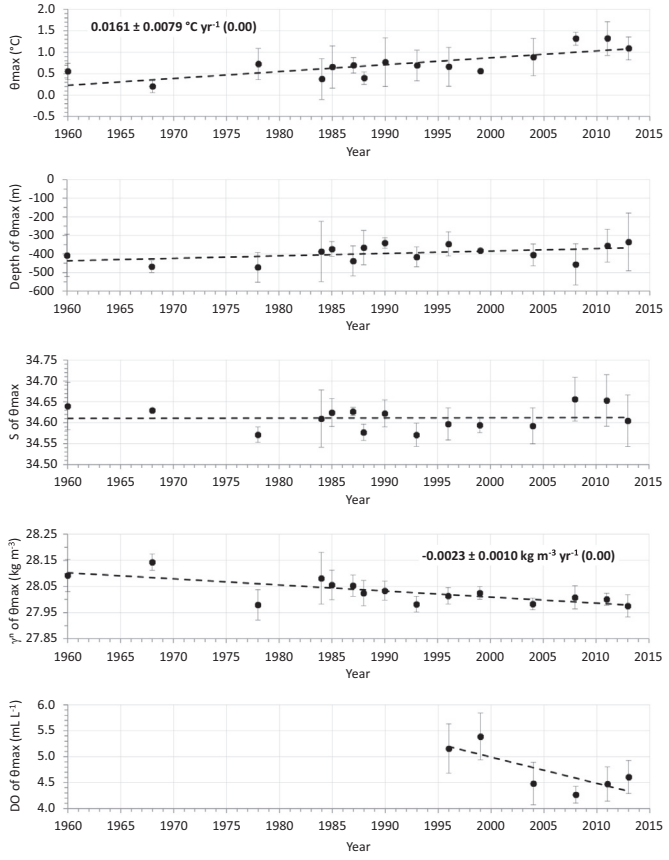

Fig. 4. Temporal evolution of the (a) maximum potential temperature, θmax, for waters with mCDW characteristics ($\theta \geq 0\,^{\circ}C$, $S \geq 34.5$ and $27.85 < \gamma^n \leq 28.27\,kg\,m^{-3}$) and profiles deeper than 500 m in the Western Basin. The θmax values were obtained below 150 m depths. Spring/summer mean with at least two observations per year are displayed with black dots. Idem for (b) depth, (c) salinity (S), (d) neutral density (γ^n) and (e) dissolved oxygen (DO) of the θmax. Vertical bars represent one standard deviation around the means. Linear fits are shown with a dashed line. Trend and confidence level in bold are statistically significant at the 95% level.

Table 1
Hydrographic trends and confidence bounds referred to θmax in the Western and Central basins. P-Values are shown in parentheses. Bold font indicates a statistically significant trend at 95% level.

Trends	Western Basin (1960–2013)	Central Basin (1963–2013)
θmax ($^{\circ}C\ yr^{-1}$)	**0.0161 ± 0.0079 (0.00)**	−0.0001 ± 0.0069 (0.98)
Depth of θmax ($m\ yr^{-1}$)	1.30 ± 2.94 (0.11)	−0.45 ± 2.52 (0.65)
S of θmax (yr^{-1})	0.0000 ± 0.0011 (0.95)	**−0.0014 ± 0.0006 (0.00)**
γ^n of θmax ($kg\ m^{-3}\ yr^{-1}$)	**−0.0023 ± 0.0010 (0.00)**	**−0.0016 ± 0.0009 (0.00)**
DO of θmax ($mL\ L^{-1}\ yr^{-1}$)	−0.0505 ± 0.1084 (0.07)	0.0109 ± 0.0369 (0.33)

3.3. Temporal variability in the intermediate and deep waters of the Western Basin (1981–2014)

All the observations collected for waters deeper than 500 m and $\gamma^n > 27.85\,kg\,m^{-3}$ (depth > 150 m) in the WB between 1981 and 2014 are presented in θ/S space in Fig. 9. The location of the profiles by year is included in Fig. S3. The mCDW core showed high variability in θ, S and γ^n within the WB throughout the study period (Fig. 9). The highest θ value within the mCDW core was observed in 2011. These waters showed periods of freshening and salinification, with decrease of S between the beginning and the end of the 1980s, early 1990s and during 1997–2004. Conversely, a consistent increase of S has been observed since 2004. The difference of the θ (DO) of $\gamma^n = 28\,kg\,m^{-3}$ between the 2000–2014 and 1960–1999 periods showed warming (decrease) and a southward shift of the 0 °C isotherm (5.5 $mL\,L^{-1}$ isoline) at the western BS (Fig. 10), indicating an increase in the presence of mCDW in that region.

On the other hand, the WB deep waters showed high interannual variability and the influence of shelf waters was apparent in the colder and denser varieties, attenuated by the exchange and mixing with the waters that surround them (Fig. 11). These waters derived from the Weddell Sea enter the WB through the south-eastern canyon that connects to the Central Basin (Fig. S5). In the 1980s (except 1985), 1990, 1996 and 1999, the thermohaline properties of the cold deep waters in the WB resulted denser than $28.27\,kg\,m^{-3}$ and also presented hydrographic characteristics similar to the HSSW from the Weddell Sea (Fig. 11). Moreover, in 2014 the deeper waters reached temperature and salinity similar to those observed before the 2000s.

3.3.1. Mixing of the Western Basin intermediate and deep waters masses

We applied the OMP analysis to quantify contributions of water masses in the layers of 500–800 m and deeper than 800 m of the WB (Fig. 12**a** and **b**, respectively). Profiles made in 1999 and 2010 did not reach depths below 800 m (Fig. S3). Spring/summer means obtained showed approximately between 25% and 40% of HSSW contribution in 1996 (Fig. 12**a** and **b**) and 1999 (Fig. 12**a**). During the 2000s, the CDW contribution represented ~85% (500–800 m) and ~55–70% (> 800 m) of the total mixture of the basin. The greater CDW contribution was associated with approximately null (< 1%) contribution of the HSSW. The drastic decrease in the HSSW contribution in the early 2000s estimated by the OMP analysis is in agreement with the salinity decrease observed in the WB waters below 500 m depth during this period (Fig. 11). In 2011 and 2013, the contributions of HSSW were ~10–15% in waters deeper than 800 m (Fig. 12**b**). Thus, high interannual variability due to changes in water masses contributions is observed in the WB deeper waters between 1980s and 2010s (Figs. 11 and 12).

3.4. Coupled oceanic-atmospheric temporal variability (1981–2014)

3.4.1. Relationship between ENSO and SAM and the mCDW extent within the Bransfield Strait

Correlation coefficients among the spring/summer normalized and detrended hydrographic parameters at the core of mCDW, referred to θmax, in the intermediate waters of the WB and the ENSO and SAM of the previous months are summarized in Table 3. Most of the data between 1981 and 2014 were collected from December to February (referred here to lag 0). θmax and S of θmax were negatively correlated ($r = -0.65$ and $p = 0.02$; $r = -0.69$ and $p = 0.01$, respectively) with ENSO (Fig. 13**a-b** and Table 3). Also, γ^n of θmax was negatively correlated with ENSO with lag 2 ($r = -0.64$ and $p = 0.03$; Table 3). The highest correlations between water mass properties and ENSO are estimated at time lags between 8 and 9 months. Conversely, the highest correlations with the SAM index were observed at lags of 4–5 months, although these were not significant at the 95% level.

During years with negative ENSO phases (La Niña), the mCDW presented the maximum northeastward extension along the southern slope of the South Shetland Islands the following summer (1985, 1990, 2011; Fig. 14). This pattern was observed during both positive (2011) and negative (1985 and 1990) SAM index of the previous winter. Conversely, during positive (El Niño) and neutral ENSO phases, the mCDW was not observed or was present in patches along the South Shetland Islands slope. Thus, the ENSO phase appears to have a significant influence on the extent of CDW within the BS.

In addition, the mCDW extends farther south in the WB region during 2000–2014 (Fig. 10). That period was generally characterized by SAM positive phases (since 1998; Fig. S2a). Moreover, the mCDW further expanded within BS during positive SAM conditions and associated with negative ENSO (i.e., 2011; Fig. 14).

Table 2
Hydrographic trends and confidence bounds (at 95% level) in the neutral density (γ^n) and depth ranges used within the Western Basin. DO trends are calculated in 1981–2013 period.

Trends	$27.85 < \gamma^n \leq 28$ (kg m^{-3} yr^{-1})	γ^n (kg m^{-3} yr^{-1}) > 28		
		500–800 m layer		> 800 m layer
	1960–2013	1960–1999	1981–2013	1981–2013
θ (°C yr^{-1})	**0.0190 ± 0.0061 (0.01)**	**−0.0229 ± 0.0068 (0.01)**	**0.0344 ± 0.0094 (0.01)**	**0.0298 ± 0.0112 (0.01)**
S (yr^{-1})	**0.0018 ± 0.0008 (0.00)**	**−0.0025 ± 0.0009 (0.01)**	0.0014 ± 0.0036 (0.20)	0.0008 ± 0.0021 (0.20)
γ^n (kg m^{-3} yr^{-1})	0.0002 ± 0.0006 (0.26)	0.0001 ± 0.0043 (0.97)	**−0.0045 ± 0.0013 (0.01)**	**−0.0054 ± 0.0017 (0.01)**
DO (mL L^{-1} yr^{-1})	**−0.0468 ± 0.0190 (0.01)**	–	−0.0301 ± 0.0899 (0.27)	−0.0264 ± 0.0582 (0.09)
Trends (1981–2013)	γ^n = 27.85 kg m^{-3}	γ^n = 28 kg m^{-3}	γ^n = 28.1 kg m^{-3}	
Isopycnal depth (m yr^{-1})	**−1.88 ± 0.31 (0.02)**	**−3.89 ± 1.07 (0.01)**	**−10.19 ± 2.30 (0.02)**	
Isopycnal θ (°C yr^{-1})	**0.0217 ± 0.0005 (0.05)**	**0.0331 ± 0.0096 (0.01)**	0.0136 ± 0.0343 (0.18)	
Isopycnal S (yr^{-1})	0.0011 ± 0.0026 (0.14)	**0.0029 ± 0.0009 (0.01)**	0.0011 ± 0.0032 (0.28)	
Isopycnal DO (mL L^{-1} yr^{-1})	−0.0302 ± 0.0685 (0.10)	**−0.0471 ± 0.0129 (0.01)**	−0.0316 ± 0.0755 (0.13)	

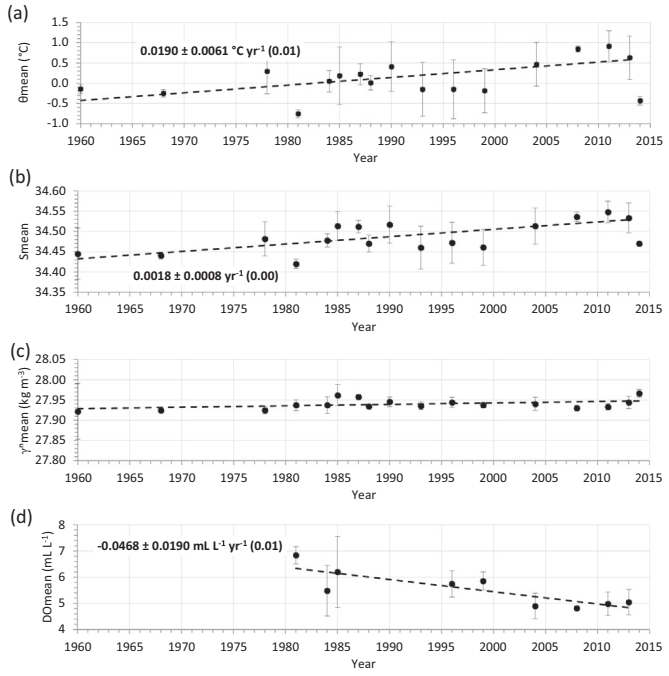

Fig. 5. Same as in Fig. 4 but for time series of the spring/summer mean of (a) potential temperature (θmean), (b) salinity (Smean), (c) neutral density (γ^nmean) and (d) dissolved oxygen (DOmean). Data were selected from the less dense intermediate waters ($27.85 < \gamma^n \leq 28$ kg m^{-3} and depths > 150 m) in the Western Basin.

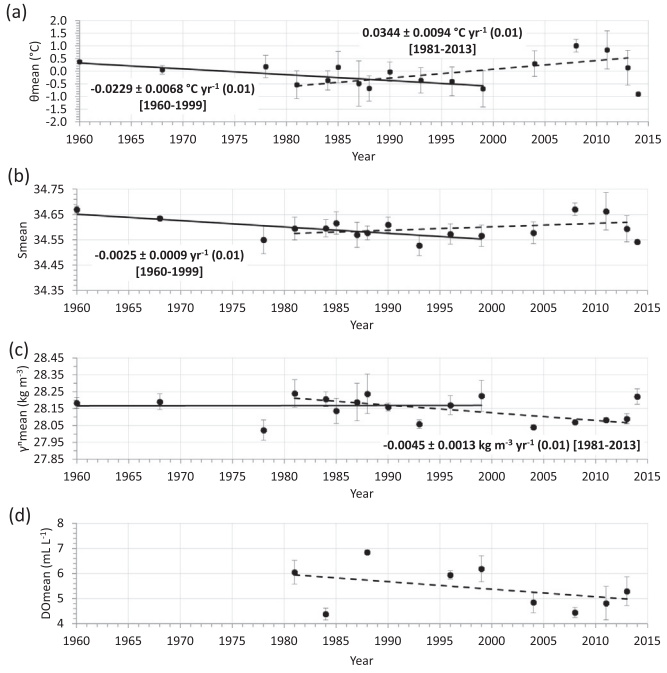

Fig. 6. Same as in Fig. 5 but for the depth range of 500–800 m. Linear fits for 1960–1999 (solid) and 1981–2013 (dashed) are shown.

3.4.2. Relationship between ENSO and SAM and the mean hydrographic properties in the intermediate and deep waters of the Western Basin

For each of the 3 layers in which the WB was divided, we tested the correlations between the detrended and normalized mean spring/summer thermohaline properties and the ENSO and SAM of the previous months. The most interesting results were obtained in the deep waters, at depths > 800 m (Table 3). The θ and S variations were negatively correlated with the April-June-averaged ENSO of the previous year, with correlation coefficients of r = −0.59 (p = 0.05) and r = −0.69 (p = 0.01), respectively (Fig. 15**a**). On the other hand, θ and S were negatively correlated with the SAM index at 4 months lag (Fig. 15**b**), with correlation coefficients of −0.63 and −0.64, respectively. Both correlations are statistically significant at 95% confidence level.

The influence of ENSO and SAM in the WB deeper water properties were analyzed in θ-S space using detrended spring/summer mean data. During the negative ENSO phase more saline and dense waters were observed, while during the positive ENSO phase S and γ^n were the lowest (Fig. 16). Also, during the negative SAM phase the most saline and dense waters were observed. The mean S in 1993 (during positive SAM and ENSO phases) was the lowest in this period. In addition, although in 2014 (negative SAM phase) no observations are available below 800 m depth, its deeper and denser waters were occupied by a saline variety of shelf waters (Fig. 11). Thus, between 1981 and 2014 the WB deep waters were in general more saline and denser during negative ENSO and SAM phases.

4. Discussion

To the best of our knowledge no long-term (interannual to interdecadal) trends in the hydrographic properties of the intermediate and deep waters of the WB of the BS have been reported in the literature. Significant total changes estimated in this study in the thermohaline properties in the Western and Central basins (Tables 1 and 2) were larger than the instrumental accuracy (see Section 2.1) and greater than ± 0.0005 yr^{-1} for S, thus considered a significant change in the ocean (Boyer et al., 2005, 2013; Azaneu et al., 2013; Dotto et al., 2016). This throws confidence in inferring that the trends obtained in this study represent robust changes. High interannual variability in the analyzed parameters was present throughout the study period, which is

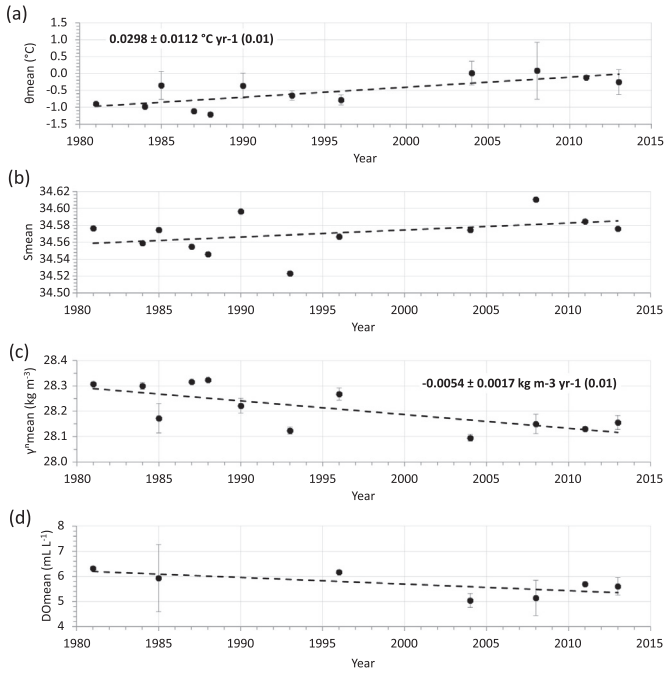

Fig. 7. Same as in Fig. 5 but for waters deeper than 800 m. Note that the time scale begins in 1980.

in agreement with several previous studies in the BS (e.g., Wilson et al., 1999; Garcia and Mata, 2005; Dotto et al., 2016). However, because the temporal and spatial distribution of oceanographic stations was not uniform within the basin, results obtained in this work should be taken with caution. There is a lack of observations in the northern part of the WB during several years (Fig. S3). Due to the more uniform thermohaline properties below 800 m (e.g., Gordon et al., 2000; Dotto et al., 2016); the trends and variability in deeper waters are generally more robust. The observed long-term trends and the interannual variability will be discussed in the following subsections.

4.1. Long-term trends

4.1.1. Trends in the mCDW core

It has been suggested that the heat flux from the CDW to the upper layers on the WAP continental shelf has increased since the 1990s (Ducklow et al., 2007). This could be a consequence of an increase in the core temperature of the CDW. Gille (2002) reported warming of 0.2 °C during 1990s in intermediate waters of the Antarctic Circumpolar Current. Also, Gille (2008) showed that the warming observed in the upper 1000 m of the Southern Hemisphere Ocean since the 1950s is concentrated in the Antarctic Circumpolar Current. In turn, Schmidtko et al. (2014) documented a significant warming (0.1 °C decade^{-1}) and few significant variations in S of CDW in most regions around Antarctica. In the Weddell Sea basin, Robertson et al. (2002) found warming of the Warm Deep Water within Weddell Gyre between 1970s and 1990s, while Von Gyldenfeldt et al. (2002) reported warming and salinification in the Warm Deep Water in the Philip Passage between Weddell and Scotia seas. In this work, we found a significant warming in the mCDW core within WB from 1960 to 2013 (Table 1), which is consistent with those studies. The S did not show significant changes during that period. Therefore, the decrease of γ^n found in the mCDW core in the WB appears to be associated with warming.

A general shoaling of the CDW core (30 m decade^{-1}) around Antarctica was reported by Schmidtko et al. (2014). That study found the highest trends in the Amundsen and Bellingshausen Seas (+50 ± 18 m decade^{-1}), the regions with the largest warming, and deepening in the northern part of the Weddell Sea, where the depth of

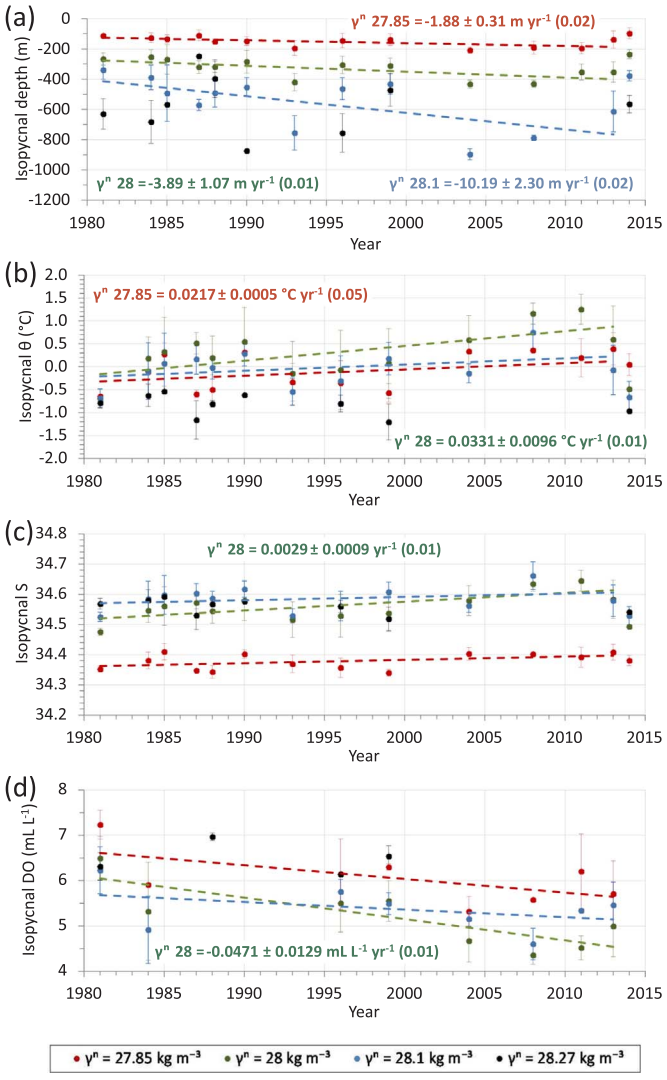

Fig. 8. (a) Temporal evolution of γ^n = 27.85 kg m^{-3}, γ^n = 28 kg m^{-3}, γ^n = 28.1 kg m^{-3} and γ^n = 28.27 kg m^{-3} isopycnal depths for profiles deeper than 500 m in the Western Basin. Vertical bars represent one standard deviation around the means. Isopycnal colors references are included in the lower bar. Linear fits (dashed lines) indicate the averaged values of γ^n = 27.85 kg m^{-3} (red), γ^n = 28 kg m^{-3} (green) and γ^n = 28.1 kg m^{-3} (blue) statistically significant (at 95% level) between 1981 and 2013. Idem for the (b) potential temperature (θ), (c) salinity (S) and (d) dissolved oxygen (DO) of each isopycna. (For interpretation of the references to color in this figure legend, the reader is referred to the web version of this article.)

CDW is correlated with cooling. In the WB of the BS, we found a shoaling signal of the θmax depth in 1960–2013, although it was not statistically significant (Fig. 4**b** and Table 1), probably due to the intense variability observed in the area (i.e., deepening observed between 1985 and 2010). Strengthened westerlies associated with the positive SAM trend since the 1960s (e.g., Marshall, 2003) can displace the Southern Antarctic Circumpolar Current front (SACCF) and Boundary (SB) closer to the Antarctic Peninsula (Renner et al., 2012). This could lead to a more intense CDW upwelling near the coasts of the Antarctic continent and hence an increasing flow of CDW onto the shelf breaks (Jacobs, 2006; Schmidtko et al., 2014).

Cooling, freshening and lightening in deeper waters of the Eastern and Central basins of the BS since the 1960s has been reported by several studies (e.g., Wilson et al., 1999; Garcia and Mata, 2005; Azaneu et al., 2013; Dotto et al., 2016). In our study, we found significant freshening and lightening in the mCDW core between 1963 and 2013 in the Central Basin (Table 1), which is consistent with those previous studies. Thus, in the Central Basin, the intermediate layer is

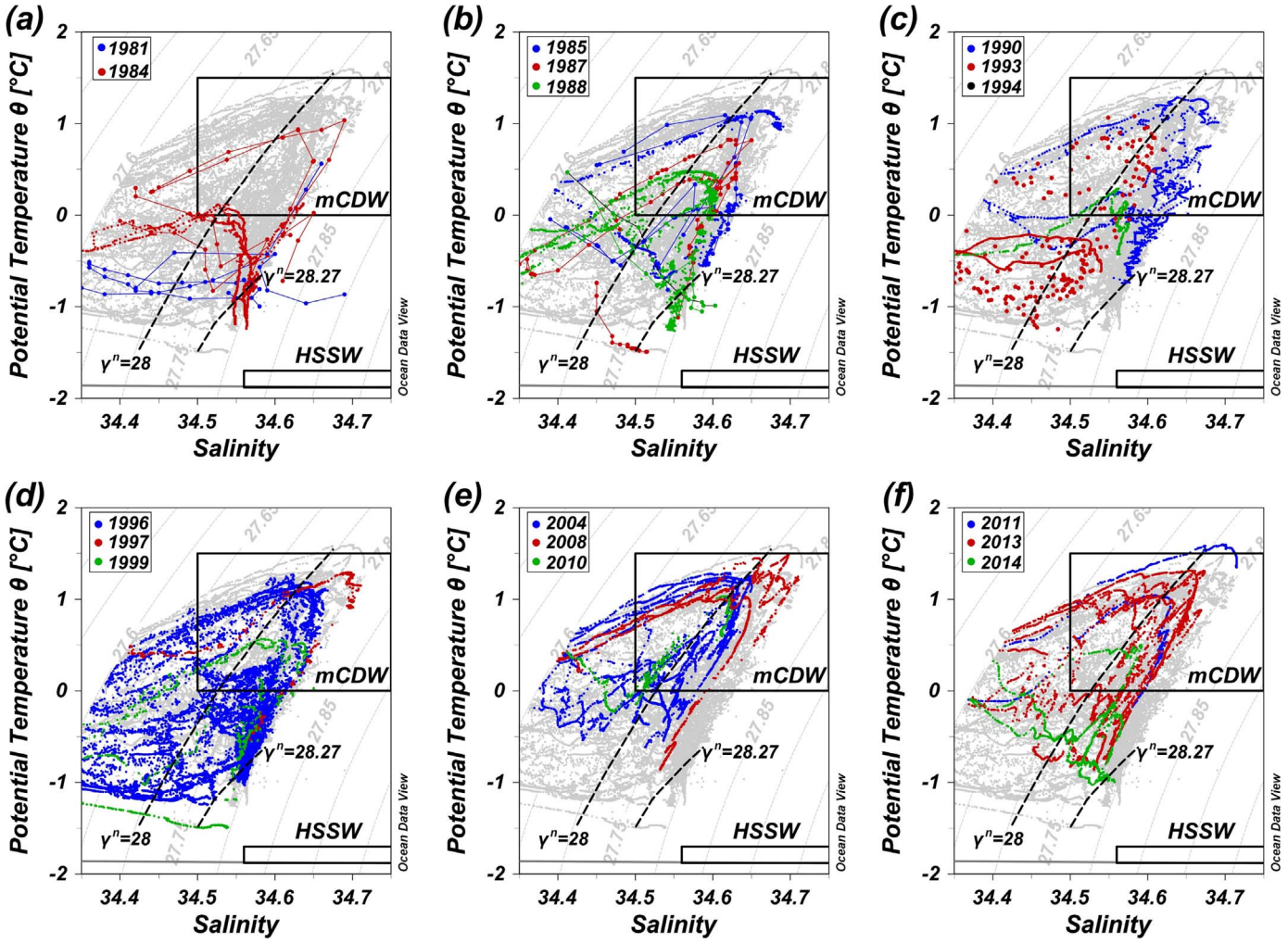

Fig. 9. θ-S diagrams for waters deeper than 500 m and $\gamma^n > 27.85\,kg\,m^{-3}$ (depth > 150 m) in the Western Basin. All the remaining data in each plot are included in light gray. Annual colors references are included in each panel. Rectangles represent modified Circumpolar Deep Water (mCDW) and High Salinity Shelf Water (HSSW). In each panel dashed lines are neutral (γ^n; black) and potential (σ0; light gray) density anomalies and the gray continue line represent the freezing point of sea water.

much influenced by cold and fresh signal from the ice shelf melting in the Weddell Sea.

4.1.2. Trends in the intermediate and deep waters of the Western Basin

Trends obtained in the neutral density range of $27.85 < \gamma^n \leq 28\,kg\,m^{-3}$, which represent intermediate waters less influenced by waters derived from the Weddell Sea, showed increase in θ and S between 1960 and 2013 (Table 2). The WB waters close to the surface layer could be influenced by the surface waters entering from the Bellingshausen Sea (i.e., TBW) and which might explain the observed variations. Increasing water temperature (> 1 °C) and salinity (> 0.25) in surface waters of the WAP in the second part of the 20th century (from 1955 to 1998) has been reported previously (Meredith and King, 2005). Warming of surface waters in summer is associated to great reduction of sea ice extension during the previous winter (Jacobs and Comiso, 1997; Meredith and King, 2005). Due to the reduction of the duration of sea ice season, a 40% reduction in mean annual sea ice extent has been recorded between the mid-1970s and late 1990s in the Bellingshausen and Amundsen seas (Jacobs and Comiso, 1997; Smith and Stammerjohn, 2001). In this work, we found a significant warming ($0.0217 \pm 0.0005\,°C\,yr^{-1}$) of the $\gamma^n = 27.85\,kg\,m^{-3}$ isopycnal (Table 2), which could be considerate representative of the surface layer in the WB. Moreover, changes in surface temperature could rapidly penetrate to deeper waters due to deep mixing, low stratification and advection along tilted isopycnals (Gille, 2008). Another hypothesis suggested, as a consequence of the increased CDW shoaling in the WB mentioned above, is that the increased CDW transport within the continental shelf enhances the vertical mixing and the heat transport to shallower waters (Dinniman et al., 2012). Moreover, the increased CDW shoaling should be associated with an increase in both the number of ice shelves and the area on each ice shelf affected by warm water (e.g., Schmidtko et al., 2014). Consequently, the spatial extent of basal melting should be increased and the ice shelf should be reduced in this region of the WAP. These waters (between $27.85 < \gamma^n \leq 28\,kg\,m^{-3}$) did not show variations of γ^n during 1960–2013, although the section of the time series between 1960 and 1996 presented a significant increase (not shown). In terms of density, the warming of these waters since the 2000s could be compensating the increase of density by salinification.

Our study also shows cooling and freshening in the depth range of 500–800 m between 1960 and 1999 (Table 2). These trends would be due to the greater influence of the Weddell Sea shelf waters in the intermediate and deep layers of the WB during that period. Passages deeper than 500 m connect the Western and Central basins, allowing the entry to the WB of the deepest and densest shelf waters originated in the Weddell Sea (Fig. S5). However, when the full period (1960–2013) is considered the trends were not significant, probably due to a trend reversal during the 2000s. The warmer, more saline, less dense and less oxygenated waters observed in the 2000s would explain these trends. This change in the hydrographic properties could be associated with an increase (decrease) of mCDW (Weddell Sea shelf waters), as discussed

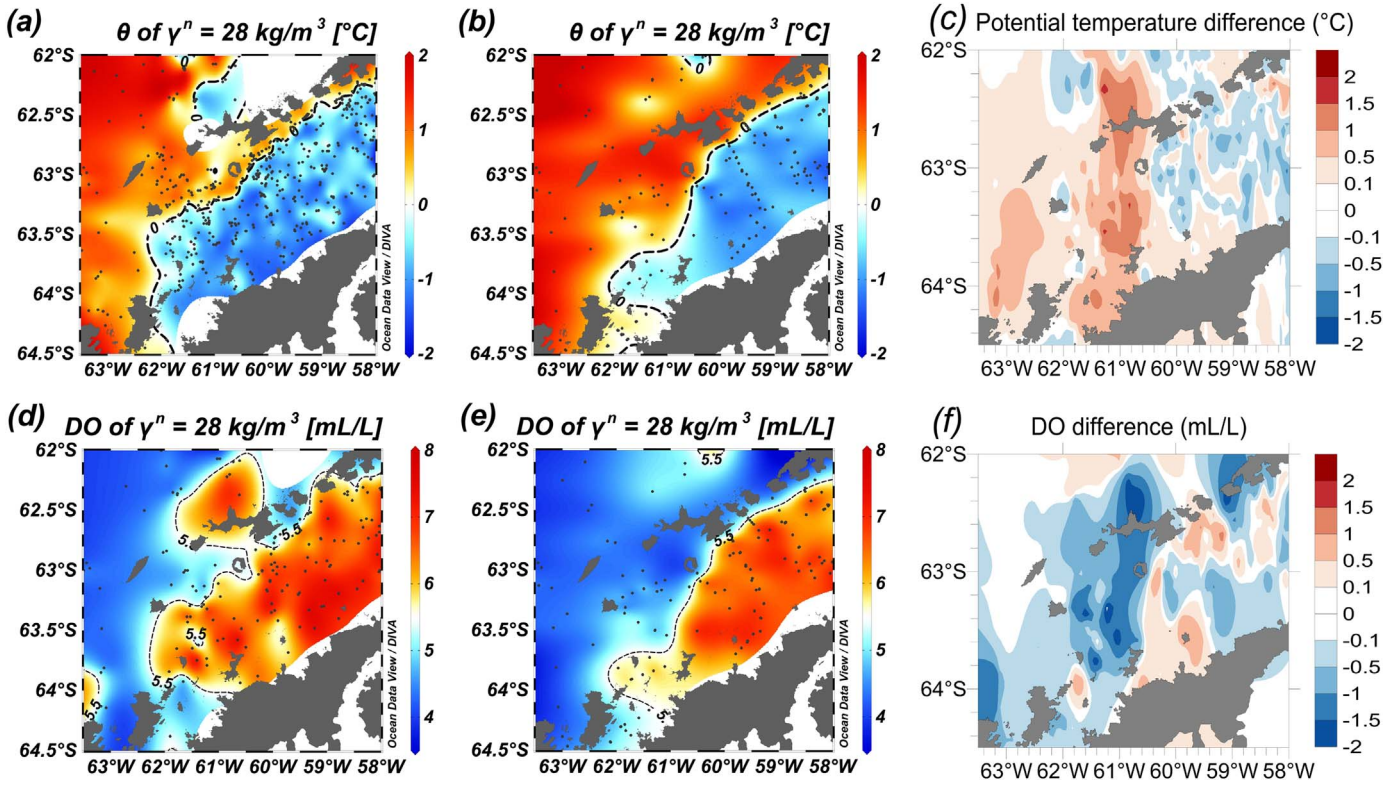

Fig. 10. Distribution of the θ (upper panel) and DO (bottom panel) along the isopycnal surface of $\gamma^n = 28\,kg\,m^{-3}$ for the (a,d) 1960–1999 period, (b,e) 2000–2014 and (c,f) difference between both periods, respectively. The dashed black line represents the 0 °C isotherm in upper panels and 5.5 mL L^{-1} in bottom panels. Data points are indicated by black dots. This dataset includes data collected between November and March from the NODC and PANGAEA dataset around Bransfield Strait.

in Section 4.2. However, if we only considered the period of time between 1981 and 2013, a significant increase in θ and a decrease in γ^n were found for the waters deeper than 500 m in the WB (Table 2). Regions around Antarctica, such as the Bellingshausen and Amundsen Seas, where the CDW core both slopes upward approaching the shelf break and is shoaling over time, showed warming in their bottom waters (Schmidtko et al., 2014). Thus, CDW changes in the Drake Passage are probably more likely to be transmitted into the WB and influence its deep waters (Schmidtko et al., 2014).

Dotto et al. (2016) suggest that the Central and Eastern basins deep waters shrinking volumes appear to be linked to freshening and lightening. Those authors suggest that there is not significant DO change due to the unchanged overall denser water masses formation rate (e.g., Van Wijk and Rintoul, 2014). In this paper, a significant DO reduction in the WB intermediate waters (which are less influenced by shelf waters; Fig. 5**d** and Table 2) suggests a change in the ventilation rate between 1981 and 2013. However, this trend is still not well determined because of the limited number of observations. Moreover, the 27.85, 28 and 28.1 $kg\,m^{-3}$ isopycnals in the WB shrank between 1981 and 2013 (Table 2), and the shrinking was more pronounced until 2004 (Fig. 8**a**), which suggests that shelf waters contribution from the Weddell Sea decreased during that period. That was compensated by expansion of CDW and surface waters, similar to what was observed in the Australian Antarctic Basin (Van Wijk and Rintoul, 2014).

The connection between the retreat of the sea ice field and changes in air pressure and temperature in the Antarctic Peninsula suggest an atmospheric control in the ice shelf retreat (Morris and Vaughan, 2003), although the thinning of the ice shelf may be a result of changes in the surface water as a "pre-condition" to the atmospheric warming, which is one of the main drivers of regional sea ice retreat (Cook and Vaughan, 2010). Changes in air-sea heat fluxes or horizontal advection of ocean heat could cause changes in the heat content of the upper ocean such as appears to have occurred in the WB water column, which could influence and respond to changes in air temperature (Gille, 2008). Initially driven by strengthening westerlies, atmospheric warming and lower increase in sea ice production (related to the positive SAM trend), these changes would act as positive feedbacks, promoting further warming and S increase in the surface waters in summer over the WAP area.

4.2. Temporal variability in the Bransfield Strait water masses and their links with modes of climate variability (1980s-2010s)

4.2.1. Temporal variability on the spatial distribution of mCDW core in the Bransfield Strait

We found significant negative correlations between the normalized and detrended thermohaline parameters of mCDW core of the WB with ENSO (Table 3). Therefore, our results showed increased θ and S values during La Niña conditions, associated with increased input of warmer mCDW to the WB. An 8–9 months lag in the response of these correlations appears reasonable compared with the ~6 months reported by Meredith et al. (2008) based on the correlation between sea surface temperature and ENSO in the Scotia Sea. Wilson et al. (1999) noted that CDW is sometimes present in the BS associated with great interannual variability. Some studies have reported the presence of mCDW patches in the Strait (Clowes, 1934; Gordon and Nowlin, 1978), while others reported it as a narrow strip carried by the Bransfield Current along the southern shelf break of the South Shetland Islands (e.g., Capella et al., 1992; Hofmann et al., 1996; Sangrà et al., 2011, 2017). We observed a similar interannual variability in the mCDW presence along the BS, which appears to be associated with ENSO phases. During La Niña conditions, the mCDW extended along the South Shetland Islands shelf break, while during El Niño conditions this warm water was observed in the Central Basin region in the form of patches, or was absent (Fig. 14). Loeb et al. (2009) found westward displacement of SACCF and SB around Elephant Island (see location in Fig. 1) during the 1990–1994

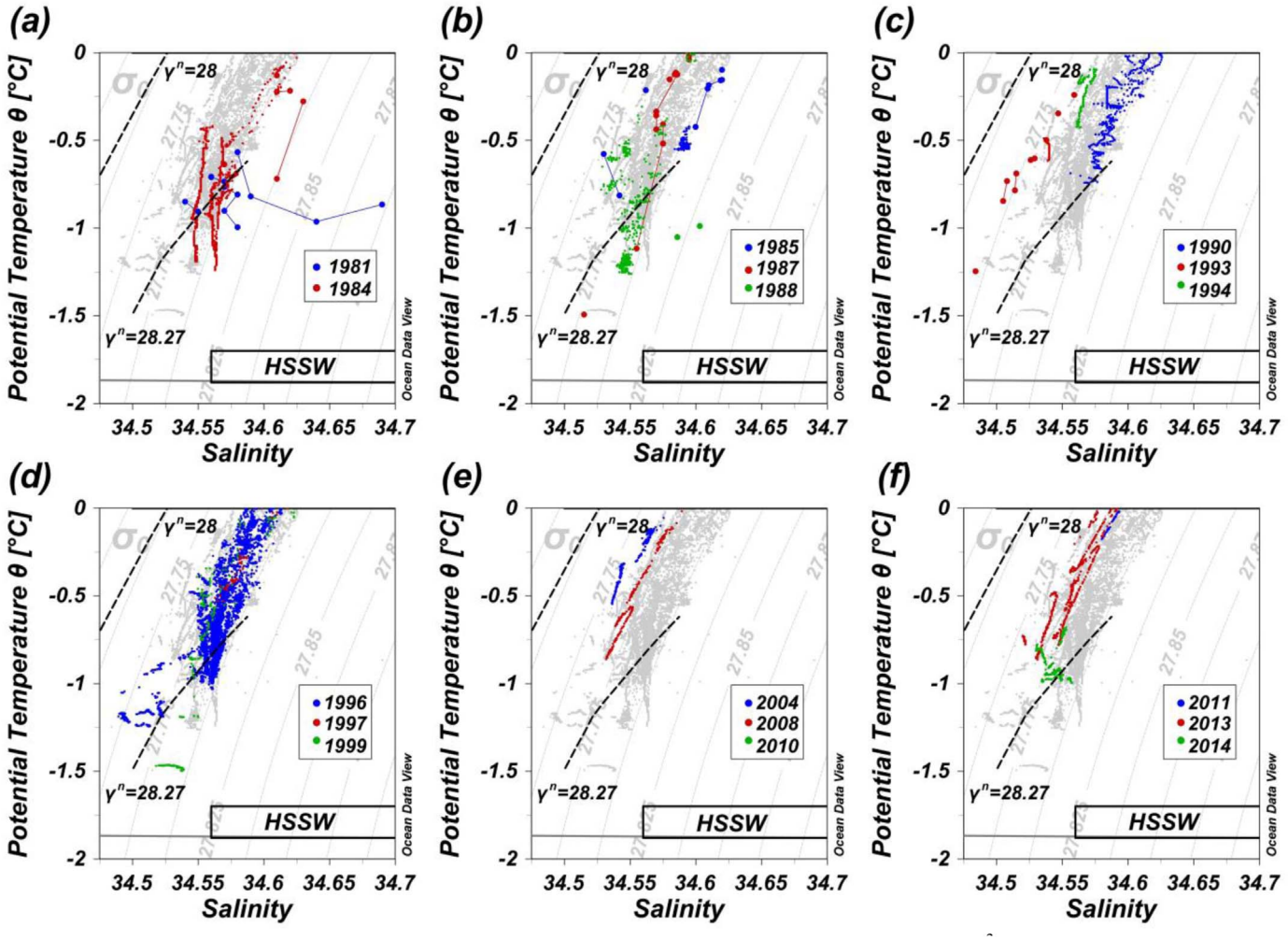

Fig. 11. Same as in Fig. 9 but for the coldest ($\theta \leq 0\,^{\circ}C$) and densest ($\gamma^n > 28.1\,kg\,m^{-3}$) deep waters (depth > 500 m).

and 1998 El Niño phases. On the other hand, they found an eastward displacement during the 1996 and 1999–2004 La Niña or neutral conditions. Thus, our results are in agreement with the pattern found by Loeb et al. (2009) in a region neighboring.

On the other hand, during positive SAM phases the westerlies increase throughout the region around the Antarctic Peninsula, pushing the SACCF and SB southward (e.g., Marshall et al., 2004; Renner et al., 2012). During the period 2000–2014, warming and DO decrease of the 28 kg m^{-3} isopycnal and a southward shift of the 0 °C isotherm and 5.5 mL L^{-1} isoline were observed within the WB (Fig. 10). Thus, the mCDW within the WB could propagate further to the south during persistent positive SAM phases due to the weakening of the current bordering the WAP (Renner et al., 2012). Fogt et al. (2011) found that when SAM and ENSO are in phase, the ENSO teleconnection to the South Pacific is stronger, and when they are out phase the teleconnection is significantly weakened or absent. When both modes are in phase, during La Niña and positive SAM phases, the advection of mCDW within BS is enhanced, which is associated with a weakening of the transport of shelf waters along the WAP, as is observed in 2011 (Fig. 14).

4.2.2. Temporal variability in the intermediate and deep waters of the Western Basin

The intermediate and deep waters in the WB presented high interannual variability in the hydrographic properties between 1981 and 2014, which potentially reflects the influence of modes of climatic variability such as ENSO and SAM. In this work, we also found negative correlations between θ and S in the WB (> 800 m depth) with ENSO and SAM (Table 3). As mentioned in Section 4.1, changes in CDW properties could be reflected in the WB bottom waters. Also, the input of mCDW to the WB increases during the La Niña phase. Thus, the deepest waters were more saline and dense under La Niña conditions; while freshening and lightening were observed in years with El Niño conditions (Figs. 15**a** and 16).

Years with more saline deep waters were found in the WB during negative SAM phases, while less saline conditions were observed during positive SAM phases (Figs. 15**b** and 16). Dotto et al. (2016) found significant negative correlations between S and γ^n in the deeper and denser waters of the Central and Eastern basins with the SAM index of the previous winter. In addition, the response time (~4 months lag) between the SAM phase at the beginning of austral spring and changes in the thermohaline parameters in summer is in agreement with the findings of Dotto et al. (2016). During negative SAM conditions denser shelf water intrusions from Weddell Sea (HSSW) flow southwestward along the Northern Antarctic Peninsula (e.g., Renner et al., 2012; Van Caspel et al., 2017) to the Central Basin of the BS (Dotto et al., 2016) and could be carried towards the WB through the south-eastern canyon, which communicates with the Central Basin (Fig. S5a).

The period 1980–1996 (and particularly 1985–1990) was characterized by intense and/or prolonged El Niño events (Fig. S2b), and was heavily influenced by atmospheric warming and declining sea ice extent around the Antarctic Peninsula (e.g., Martinson et al., 2008; Loeb et al., 2009). Waters in the 500–800 m layer showed decreases in θ and S until 1999 (Fig. 6**a** and **b**). This period was characterized by the

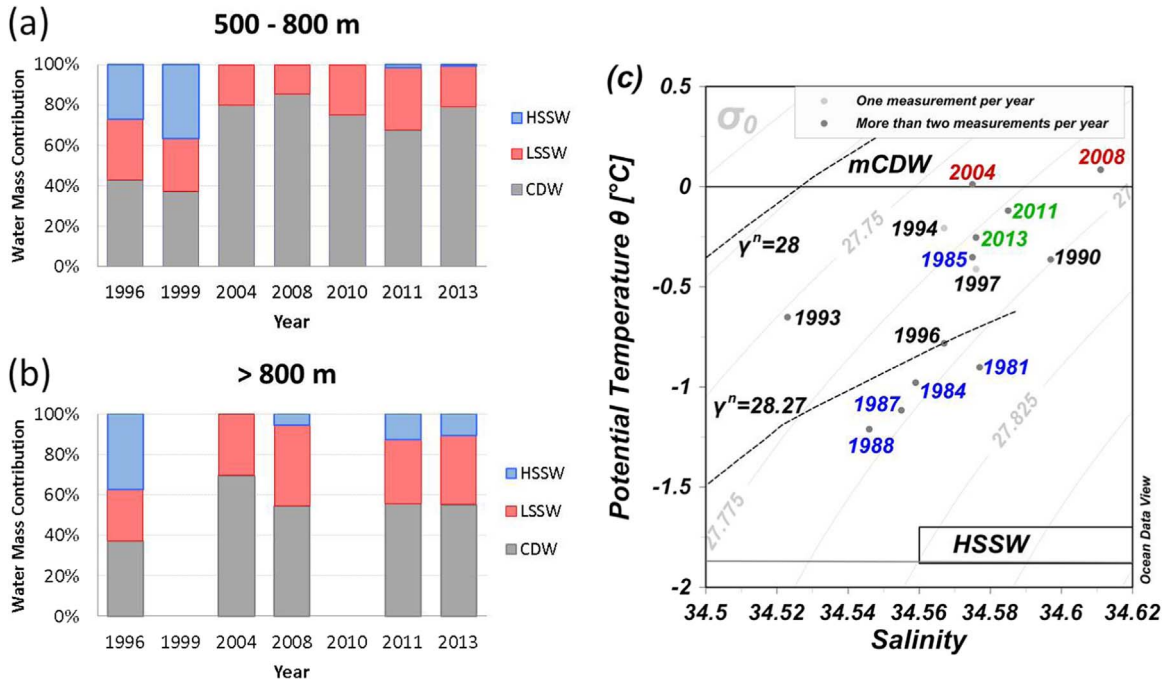

Fig. 12. Temporal evolution of the spring/summer mean proportions of distinct water masses within the water column in (a) 500–800 m layer and (b) below 800 m in the WB. The mean proportions were calculated with the OMP analysis for years between 1996 and 2013. CDW = Circumpolar Deep Water (gray), LSSW = Low Salinity Shelf Water (red), HSSW = High Salinity Shelf Water (blue). (c) θ-S diagrams time of the spring/summer averages for waters deeper than 800 m between 1980 and 2013. Values are classified by 1980s (blue), 1990s (black), 2000s (red) and 2010s (green). (For interpretation of the references to color in this figure legend, the reader is referred to the web version of this article.)

Table 3
The normalized and detrended hydrographic properties referred to θmax value correlations with the ENSO and SAM (3-month moving averaged) of the previous months in the Western Basin (1981–2014). Below, same as above but for the mean values of the hydrographic properties obtained below 800 m depth. It is indicated the lag value of the best correlation. Lag 0 = December-February, Lag 1 = November-January and successively. Significant correlation at 95% confidence level is indicated by bold type.

ENSO vs θmax	ENSO vs S of θmax	ENSO vs γ^n of θmax	SAM vs θmax	SAM vs S of θmax	SAM vs γ^n of θmax
−0.65 (0.02)	**−0.69 (0.01)**	**−0.64 (0.03)**	−0.45 (0.14)	−0.31 (0.33)	0.40 (0.20)
Lag 9	**Lag 8**	**Lag 2**	Lag 4	Lag 4	Lag 2
Correlation coefficients for Western Basin water column below 800 m depth.					
ENSO vs θ	ENSO vs S	ENSO vs γ^n	SAM vs θ	SAM vs S	SAM vs γ^n
−0.59 (0.05)	**−0.69 (0.01)**	0.27 (0.40)	**−0.63 (0.03)**	**−0.64 (0.03)**	−0.55 (0.06)
Lag 8	**Lag 8**	Lag 6	**Lag 4**	**Lag 4**	Lag 0

presence of bottom water denser than 28.27 kg m^{-3} during several years (Figs. 3**c** and 11), which indicates the dilution of shelf waters originating in the Weddell Sea.

Since 1990, strong teleconnections were found between ENSO and SAM (Fig. S2b): generally La Niña occurred during the positive SAM phase and El Niño occurred during the negative SAM phase (Fogt and Bromwich, 2006; Stammerjohn et al., 2008). During the 1990s, the θ and S in the 27.85 < γ^n ≤ 28 kg m^{-3} layer were relatively low and did not show changes during the years when data are available (Fig. 5**a** and **b**). This was a period of relatively stable sea ice conditions in the WAP area (Loeb et al., 2009). In the other hand, waters deeper than 500 m in the WB were marked by cooling and increase of S and γ^n (Figs. 11 and

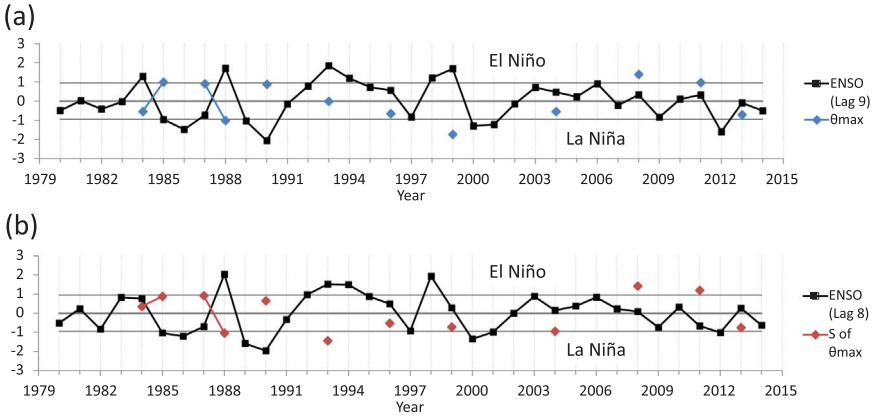

Fig. 13. Temporal evolution of the standardized (a) θmax (blue) and (b) S(θmax) (red) in the Western Basin and the BEST index (ENSO). ENSO (black) is the average of April–June (Lag 8) and March–May (Lag 9) of each year. ENSO is advanced one year for better comparison. (For interpretation of the references to color in this figure legend, the reader is referred to the web version of this article.)

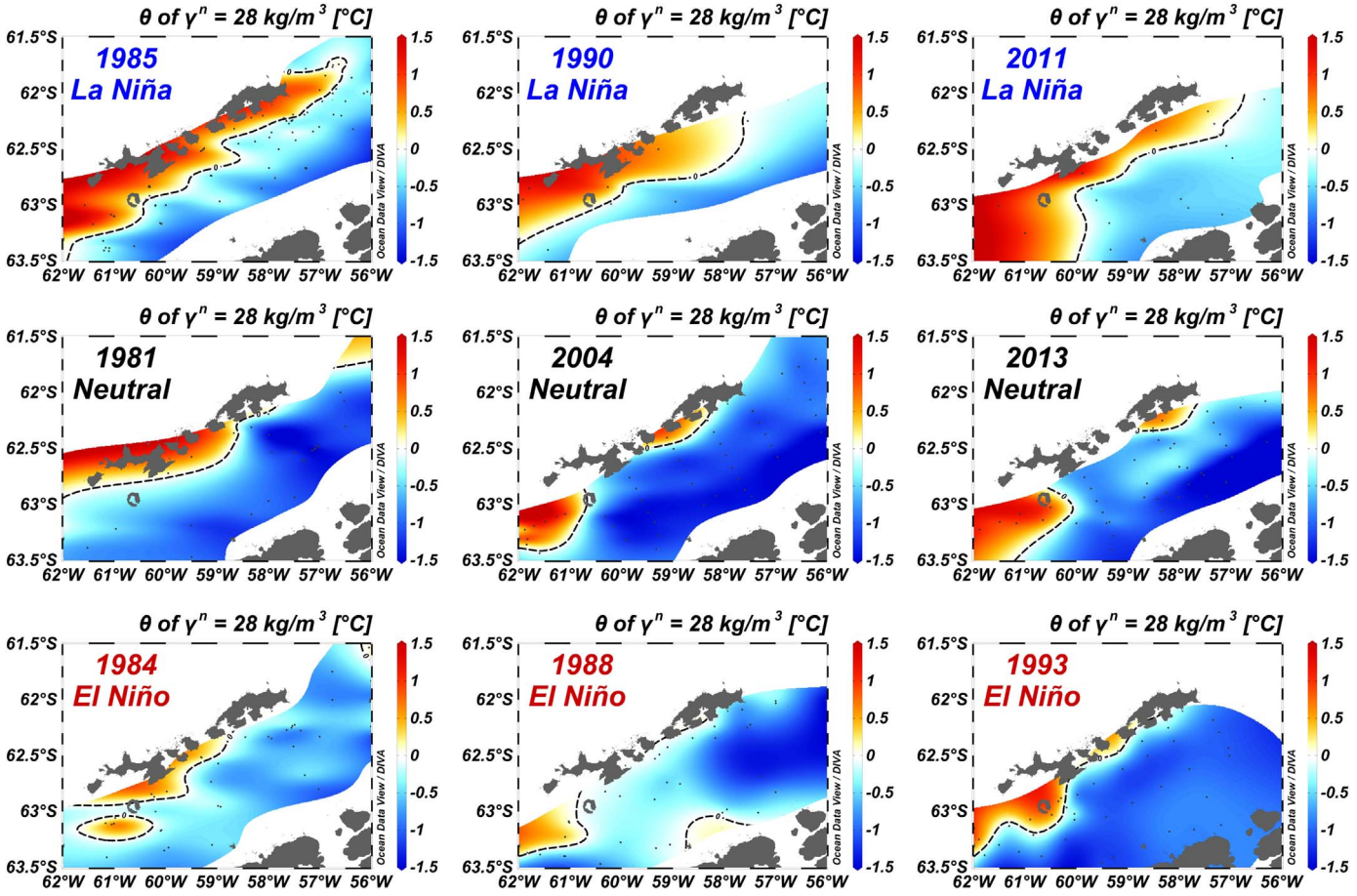

Fig. 14. Spatial distribution of θ along the isopycnal surface of $\gamma^n = 28\ kg\ m^{-3}$ in the Bransfield Strait. The sign of the phase of ENSO and the spring/summer are indicated in each plot: La Niña (upper panel), Neutral (middle panel) and El Niño (lower panel). The dashed black line represents the 0 °C isotherm.

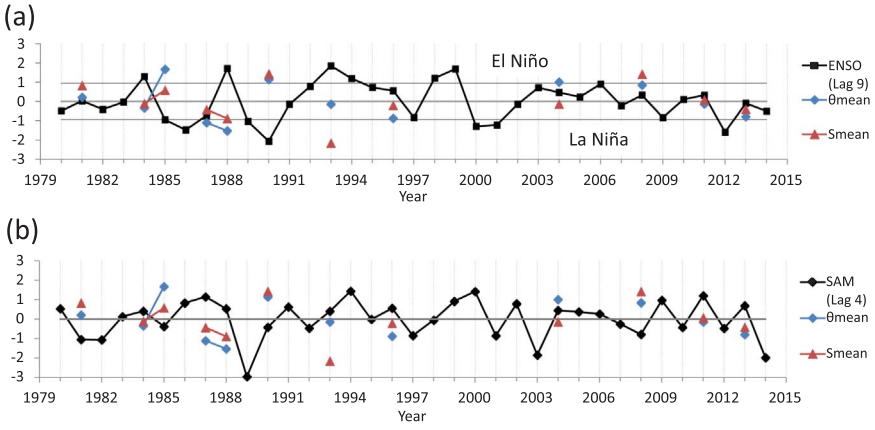

Fig. 15. Same as in Fig. 12 but for the θmean (blue) and Smean (red) of the Western Basin deeper waters (depth > 800 m) and the (a) ENSO and (b) the SAM index. ENSO and SAM are in black. ENSO is the average of March-May (Lag 9) and the SAM is the average of August-October (Lag 4) of each year. (For interpretation of the references to color in this figure legend, the reader is referred to the web version of this article.)

12) due to low contribution of mCDW and greater influence of HSSW.

Since 1998, stronger and more prolonged La Niña events have been present, while weaker or less prolonged El Niño events were reported for the same period (Fig. S2b). In general, positive SAM conditions were present over this period (Fig. S2). During the 2000s, both the mCDW core in the western BS and the 27.85–28 kg m^{-3} γ^n layer within the WB, were characterized by warming, salinification and DO reductions (Figs. 4 and 5). The simultaneous La Niña and positive SAM phases should favor the greater mCDW contribution in the WB waters. The deepest waters (depth > 500 m) showed increased θ values and decreased γ^n and DO values during this period (Figs. 6 and 7), which could be associated to a greater proportion of mCDW in the mixing of the WB deep waters (Fig. 12). Also, a minor HSSW contribution to the shelf waters revealed by the OMP analysis is in agreement with the lower salinity found during the 2000s (Figs. 11 and 12). Both patterns are associated to persistent positive SAM phases, during which stronger westerlies move mCDW to south and a local variety of relatively less dense shelf waters sinks into the BS.

Since 2010, a decrease (an increase) of θ and S (DO) were recorded in WB waters above 800 m (Figs. 4–6 and 9) that could be associated to a LSSW increase and a corresponding mCDW decrease (Fig. 12**a**). Also, increased S in the denser and deeper (> 800 m) waters (Fig. 11**a** and **b**) would be related to an increase in the proportion of HSSW and a reduction of mCDW in the total mixture (Fig. 12**b** and **c**). Dotto et al. (2016) found an increase of ~0.06 in S in the Central Basin deep waters during this period, and associated this observation with an increase in

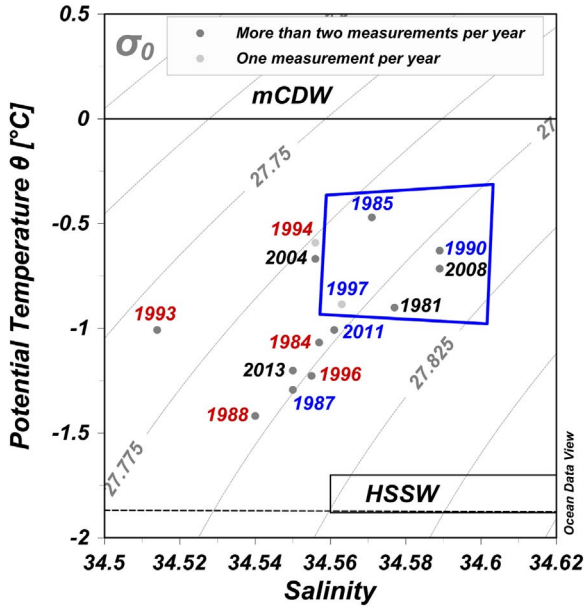

Fig. 16. θ-S of spring/summer averages below 800 m depth and detrended in the Western Basin (1981–2013). Values are classified by positive (red), neutral (black) and negative (blue) phase of ENSO. Values inside (outside) blue polygon were recorded in negative (positive) SAM phases. (For interpretation of the references to color in this figure legend, the reader is referred to the web version of this article.)

the contribution of HSSW (and reduced contribution of LSSW) of approximately 20%. Moreover, 2014 unveiled the densest waters ($> 28.27\ kg\ m^{-3}$) in the WB, not observed since 1999 (Fig. 11). Similar behavior was also reported in the other basins of the BS (Dotto et al., 2016). Finally, a monotonic shoaling of the depths of the 27.85, 28 and $28.1\ kg\ m^{-3}$ isopycnals has been observed in the WB since 2008 (Fig. 8**a**). In the 2010s, a change occurred from La Niña and positive SAM phase to neutral ENSO conditions and negative SAM phase (Fig. S2b). Turner et al. (2015) found an air temperature trend inversion since the late 1990s associated with greater east-to-southeasterly winds.

5. Summary and conclusions

In this paper, we analyzed the thermohaline variability of the Bransfield Strait Western Basin (WB) from a hydrographic data set spanning approximately five decades (1960s-2010s). We found long-term warming and lightening of the mCDW core statistically significant (95% confidence level) in the WB: $0.0161 \pm 0.0079\ °C\ yr^{-1}$ and $-0.0023 \pm 0.0010\ kg\ m^{-3}\ yr^{-1}$, respectively (1960–2013). This result is in agreement with previous findings reported in neighbor areas (e.g., Gille, 2002, 2008; Schmidtko et al., 2014). On the other hand, the mCDW core presents a decrease in S ($-0.0014 \pm 0.0006\ yr^{-1}$) and γ^n ($-0.0016 \pm 0.0009\ kg\ m^{-3}\ yr^{-1}$) in the Central Basin between 1963 and 2013. These trends are influenced by the freshening and lightening observed in Weddell Sea shelf waters (e.g., Garcia and Mata, 2005; Azaneu et al., 2013; Dotto et al., 2016).

The less dense intermediate waters ($27.85 < \gamma^n \leq 28\ kg\ m^{-3}$) of the WB experienced statistically significant (at 95% confidence level) warming and salinification at rates of $0.0190 \pm 0.0061\ °C\ yr^{-1}$ and $0.0018 \pm 0.0008\ yr^{-1}$, respectively, between 1960 and 2013. These trends could be associated with advection of heat due to warming and greater reduction of sea ice extent from Bellingshausen surface waters. Another hypothesis explaining these trends is due to heat flux from mCDW to the upper layers associated with the positive SAM trend observed since the 1960s. In addition, a significant deepening of this layer was recorded during 1981–2013 (Table 2). The 500–800 m layer in the WB presented cooling ($-0.0229 \pm 0.0068\ °C\ yr^{-1}$) and freshening ($-0.0025 \pm 0.0009\ yr^{-1}$) until late 1990s. These trends could be associated to an enhanced influence of Weddell Sea shelf water during this period. Conversely, warming and lightening were found between 1981 and 2013, both in 500–800 m and > 800 m layers (Table 2), due to reduced contribution of shelf waters and greater of mCDW within the basin. These hydrographic changes could be associated with a southward migration of marine species observed in the WAP between 1978 and 2006 (Montes-Hugo et al., 2009).

The θ, S and γ^n of the mCDW core in the WB are negatively correlated with ENSO. In negative ENSO phases (La Niña) the mCDW spreads through the Bransfield Strait along the southern slope of the South Shetland Islands (Fig. 10). During 2000–2014 (generally in positive SAM phases) the mCDW propagated southward within the WB (Fig. 14). The abrupt change in the climate regime between two well-differentiated states around 1998 had a major impact on hydrographic and biological conditions around the Antarctic Peninsula (e.g., Martinson et al., 2008; Loeb et al., 2009).

The deep waters θ and S (> 800 m) are negatively correlated with ENSO and SAM (Table 3). Warming and decrease in DO content suggests the increase (decrease) of CDW (Weddell Sea shelf waters) contribution to the deep WB during the 2000s. During the negative SAM phase the contribution of HSSW to the shelf waters increased in the WB, whereas during the positive SAM phase the contribution of LSSW increased. The same pattern was reported in the other basins of the Bransfield Strait (Dotto et al., 2016). The 1980s was a period characterized by positive ENSO phases (El Niño) and salinification in the less dense intermediate waters of the WB, associated with the substantial sea ice retreat. Also, the high proportion of shelf waters in the deeper waters of the basin reflected the freshening and lightening of waters derived from Weddell Sea in the 1980s and 1990s. Simultaneous in-phase La Niña and positive SAM events during the 2000s showed a greater contribution of mCDW in the mixing ratio. Between 2010 and 2014, the increase of HSSW contribution to the WB deeper waters is in agreement with a corresponding decrease of mCDW. Moreover, shoaling of 27.85, 28 and $28.1\ kg\ m^{-3}$ isopycnals have been observed since 2008, thus reversing the sign of the trends obtained. Therefore, the interannual observed variability in WB deep waters appears to be linked to ENSO and SAM.

The Bransfield Strait waters showed large interannual variability due to the varying influence of distinct water masses derived from different sources. The changes in the properties of mCDW reported in this work could have been caused by the regional climate change observed since the 1950s (increase in air temperature and precipitations, southward displacement of sea ice, dilution of shelf waters, positive SAM index, basal melting, etc.). Lightening due to warming associated with CDW, and freshening due to an enhanced influence of Weddell Sea shelf waters have been reported in the WB. The reduction in sea ice cover (and greater number of ice-free areas); a greater contribution of mCDW and increased upwelling; and variability in volume and the extent of glacial meltwater play critical role on the marine ecosystem, particularly on primary production (e.g., Dierssen et al., 2002; Clarke et al., 2007; Schmidtko et al., 2014).

To confirm the significant trends and interannual variations in the hydrographic properties of the WB it is necessary to continue collecting high-quality hydrographic observations, including the deployment of moorings capable of detecting the subtle changes in deep and bottom water characteristics with improved temporal resolution. To address these issues, long-term observations are also needed in the source regions of the Bransfield Strait water masses.

Acknowledgements

This study provides a contribution to the activities of the Brazilian High Latitudes Oceanography Group (GOAL), which is part of the Brazilian Antarctic Program (PROANTAR). GOAL has been funded by and/or has received logistical support from the Brazilian Ministry of the Environment (MMA), the Brazilian Ministry of Science, Technology,

Innovation and Communication (MCTIC), and the Brazilian Council for Research and Scientific Development (CNPq) through grants from the Brazilian National Institute of Science and Technology of Cryosphere (INCT-CRIOSFERA; CNPq grants n° 573720/2008-8 and 465680/2014-3), NAUTILUS (CNPq grant n° 405869/2013-4), and CAPES/CMAR2 (CAPES grant n° 23038.001421/2014-30) projects. A.R. Piola acknowledges the support of the Inter-American Institute for Global Change Research (IAI grant CRN3070) through the US National Science Foundation grant GEO-1128040. E.M. Ruiz Barlett, G.V. Tosonotto and M.E. Sierra acknowledge the support of the Instituto Antártico Argentino (IAA). M. M. Mata acknowledges CNPq researcher grant 306896/2015-0. We would also like to thank to Silvia Rodríguez, Martha Martorell, Lucas Martínez Alvarez and Alfredo Costa for providing language help.

Appendix A. Supporting information

Supplementary data associated with this article can be found in the online version at http://dx.doi.org/10.1016/j.dsr2.2017.12.010.

References

Atkinson, A., Siegel, V., Pakhomov, E., Rothery, P., 2004. Long-term decline in krill stock and increase in salps within the Southern Ocean. Nature 432, 100–103. http://dx.doi.org/10.1038/nature02996.

Azaneu, M., Kerr, R., Mata, M.M., Garcia, C.A.E., 2013. Trends in the deep Southern Ocean (1958–2010): implications for Antarctic Bottom Water properties and volume export. J. Geophys. Res.: Oceans 118, 1–15. http://dx.doi.org/10.1002/jgre.20303.

Boyer, T.P., Levitus, S., Antonov, J.I., 2005. Linear trends in salinity for the World Ocean, 1955–1988. Geophys. Res. Lett. 32, L01604. http://dx.doi.org/10.1029/2004GL021791.

Boyer, T.P., et al., 2013. World ocean database 2013. In: Levitus, S., Mishonov, A. (Eds.), NOAA Atlas NESDIS 72. Silver Spring, Md., pp. 209. http://dx.doi.org/10.7289/V5NZ85MT.

Budillon, G., Pacciaroni, M., Cozzi, S., Rivaro, P., Catalano, G., Ianni, C., Cantoni, C., 2003. An optimum multiparameter mixing analysis of the shelf waters in the Ross Sea. Antarct. Sci. 15, 105–118. http://dx.doi.org/10.1017/S095410200300110X.

Capella, J.E., Ross, R.M., Quentin, L.B., Hofmann, E.E., 1992. A note on the thermal structure of the upper ocean in the Bransfield Strait-South Shetland Islands region. Deep-Sea Res. 39 (7–8), 1221–1229. http://dx.doi.org/10.1016/0198-0149(92)90065-2.

Carleton, A.M., 2003. Atmospheric teleconnections involving the Southern Ocean. J. Geophys. Res. 108. http://dx.doi.org/10.1029/2000JC000379.

Clarke, A., Murphy, E.J., Meredith, M.P., King, J.C., Peck, L.S., Barnes, D.K.A., Smith, R.C., 2007. Climate change and the marine ecosystem of the western Antarctic Peninsula. Philos. Trans. R. Soc. Lond. B Biol. Sci. 362 (1477), 149–166. http://dx.doi.org/10.1098/rstb.2006.1958.

Clem, K.R., Fogt, R.L., 2013. Varying roles of ENSO and SAM on the Antarctic Peninsula Climate in austral spring. J. Geophys. Res.: Atmos. 118, 1–12. http://dx.doi.org/10.1002/jgrd.50860.

Clowes, A.J., 1934. Hydrology of the Bransfield Strait. Discov. Rep. 9, 1–64.

Cook, A.J., Fox, A.J., Vaughan, D.G., Ferrigno, J.G., 2005. Retreating glacier fronts on the Antarctic Peninsula over the past half-century. Science 308, 541–544. http://dx.doi.org/10.1126/science.1104235.

Cook, A.J., Vaughan, D.G., 2010. Overview of areal changes of the ice shelves on the Antarctic Peninsula over the past 50 years. Cryosphere 4, 77–98. http://dx.doi.org/10.5194/tc-4-77-2010.

Couto, N., Martinson, D.G., Kohut, J., Schofield, O., 2017. Distribution of upper circumpolar deep water on the warming continental shelf of the West Antarctic Peninsula. J. Geophys. Res. 122 (7), 5306–5315. http://dx.doi.org/10.1002/2017JC012840.

Dierssen, H.M., Smith, R.C., Vernet, M., 2002. Glacial meltwater dynamics in coastal waters west of the Antarctic Peninsula. Proc. Natl. Acad. Sci. USA 99, 1790–1795. http://dx.doi.org/10.1073/pnas.032206999.

Dinniman, M.S., Klinck, J.M., Hofmann, E.E., 2012. Sensitivity of circumpolar deep water transport and ice shelf basal melt along the west Antarctic Peninsula to changes in the winds. J. Clim. 25, 4799–4816. http://dx.doi.org/10.1175/JCLI-D-11-00307.1.

Dotto, T.S., Kerr, R., Mata, M.M., Garcia, A.E., 2016. Multidecadal freshening and lightening in the deep waters of the Bransfield Strait, Antarctica. J. Geophys. Res. 121. http://dx.doi.org/10.1002/2015JC011228.

Ducklow, H.W., Baker, K., Fraser, W.R., Martinson, D.G., Quetin, L.B., Ross, R.M., Smith, R.C., Stammerjohn, S., Vernet, M., 2007. Marine ecosystems: the West Antarctic Peninsula. Philos. Trans. R. Soc. B. 362, 67–94. http://dx.doi.org/10.1098/rstb.2006.1955.

Fahrbach, E., Hoppema, M., Rohardt, G., Schröder, M., Wisotzki, A., 2004. Decadal-scale variations of water mass properties in the deep Weddell Sea. Ocean Dyn. 54, 77–91. http://dx.doi.org/10.1007/s10236-003-0082-3.

Fogt, R.L., Bromwich, D.H., 2006. Decadal variability of the ENSO teleconnection to the high latitude South Pacific governed by coupling with the Southern Annular Mode. J. Clim. 19, 979–997.

Fogt, R.L., Bromwich, D.H., Hines, K.M., 2011. Understanding the SAM influence on the South Pacific ENSO teleconnection. Clim. Dyn. 36, 1555–1576.

García, M.A., López, O., Sospedra, J., Espino, M., Gràcia, V., Morrison, G., Rojas, P., Figa, J., Puigdefàbregas, J., Sánches-Arcilla, A., 1994. Mesoscale variability in the Bransfield Strait region (Antarctica) during Austral summer. Ann. Geophys. 12 (9), 856–867.

García, M.A., Castro, C.G., Ríos, A.F., Doval, M.D., Rosón, G., Gomis, D., López, O., 2002. Water masses and distribution of physico-chemical properties in the Western Bransfield Strait and Gerlache Strait during Austral summer 1995/96. Deep-Sea Res. II 49, 585–602.

Garcia, C.A.E., Mata, M.M., 2005. Deep and bottom water variability in the central basin of Bransfield Strait (Antarctica) over the 1980–2005 period. CLIVAR Exch. 10, 48–50.

Gille, S.T., 2002. Warming of the Southern Ocean since 1950s. Science 295, 1275–1277.

Gille, S.T., 2008. Decadal-scale temperature trends in the Southern Hemisphere Ocean. J. Clim. 21, 4749–4765. http://dx.doi.org/10.1175/2008JCLI2131.1.

Gong, D., Wang, S., 1999. Definition of Antarctic Oscillation Index. Geophys. Res. Lett. 26, 459–462.

Gordon, A.L., Nowlin Jr., W.D., 1978. The Basin Waters of the Bransfield Strait. J. Phys. Oceanogr. 8, 258–264.

Gordon, A.L., Mensch, M., Dong, Z., Smethie Jr., W.M., de Bettencourt, J., 2000. Deep and bottom water of the Bransfield Strait eastern and Central Basins. J. Geophys. Res. 105, 11337–11346 (doi:2007GL030340/2000JC900030).

Hall, A., Visbeck, M., 2002. Synchronous variability in the Southern Hemisphere atmosphere, sea ice and ocean resulting from the annular mode. J. Clim. 15, 3043–3057.

Hellmer, H.H., Huhn, O., Gomis, D., Timmermann, R., 2011. On the freshening of the northwestern Weddell Sea continental shelf. Ocean Sci. 7, 305–316. http://dx.doi.org/10.5194/os-7-305-2011.

Hofmann, E.E., Klinck, J.M., Lascara, C.M., Smith, D.A., 1996. Water mass distribution and circulation west of the Antarctic Peninsula and including Bransfield Strait. In: Ross, R.M., Hofmann, E.E., Quetin, L.B. (Eds.), Antarctic Res. Series 70. American Geophys. Union, Washington DC, pp. 61–80.

Jackett, D.R., McDougall, T.J., 1997. A neutral density variable for the world's oceans. J. Phys. Oceanogr. 27 (2), 237–263. http://dx.doi.org/10.1175/1520-0485(1997)0272.0.CO;2.

Jacobs, S.S., Comiso, J.C., 1997. Climate variability in the Amundsen and Bellingshausen Seas. J. Clim. 10, 697–709.

Jacobs, S., 2006. Observations of change in the Southern Ocean. Philos. Trans. R. Soc. Lond. A364, 1657–1681.

Kerr, R., Heywood, K.J., Mata, M.M., Garcia, C.A.E., 2012. On the outflow of dense water from the Weddell and Ross Sea in OCCAM model. Ocean Sci. 8, 369–388. http://dx.doi.org/10.5194/os-8-369-2012.

Klinck, J.M., Hofmann, E.E., Beardsley, R.C., Salihoglu, B., Howard, S., 2004. Water-mass properties and circulation on the west Antarctic Peninsula Continental Shelf in Austral Fall and Winter 2001. Deep-Sea Res. II 51, 1925–1946.

Loeb, V.J., Hofmann, E.E., Klinck, J.M., Holm-Hansen, O., White, W.B., 2009. ENSO and variability of the Antarctic Peninsula pelagic marine ecosystem. Antarct. Sci. 21 (2), 135–148. http://dx.doi.org/10.1017/S0954102008001636.

Mackas, D.L., Denman, K.L., Bennett, A.F., 1987. Least-square multiple tracer analysis of water mass composition. J. Geophys. Res. 92, 2907–2918.

Marshall, G.J., 2003. Trends in the Southern Annular Mode from observations and reanalyses. J. Clim. 16, 4134–4143.

Marshall, G.J., Stott, P.A., Turner, J., Connolley, W.M., King, J.C., Lachlan-Cope, T.A., 2004. Causes of exceptional atmospheric circulation changes in the Southern Hemisphere. Geophys. Res. Lett. 31, L14205. http://dx.doi.org/10.1029/2004GL019952.

Marshall, G.J., Orr, A., van Lipzig, N.P.M., King, J.C., 2006. The impact of a changing Southern Hemisphere Annular Mode on Antarctic Peninsula summer temperatures. J. Clim. 19, 5388–5404.

Martinson, D.G., Stammerjohn, S.E., Iannuzzi, R.A., Smith, R.C., Vernet, M., 2008. Western Antarctic Peninsula physical oceanography and spatio-temporal variability. Deep-Sea Res. II 55, 1964–1987. http://dx.doi.org/10.1016/j.dsr2.2008.04.038.

McKee, D.C., Yuan, X., Gordon, A.L., Huber, B.A., Dong, Z., 2011. Climatic impact on interannual variability of Weddell Sea Bottom Water. J. Geophys. Res. 116, C05020. http://dx.doi.org/10.1029/2010JC006484.

Meredith, M.P., King, J.C., 2005. Rapid climate change in the ocean west of the Antarctic Peninsula during the second half of the 20th century. Geophys. Res. Lett. 32, L19604 (doi:2007GL030340/2005GL024042).

Meredith, M.P., Murphy, E.J., Hawker, E.J., King, J.C., Wallace, M.I., 2008. On the interannual variability of ocean temperatures around South Georgia, Southern Ocean: forcing by El Niño/southern oscillation and the southern annular mode. Deep-Sea Res. II Top. Stud. Oceanogr. 55 (18–19), 2007–2022. http://dx.doi.org/10.1016/j.dsr2.2008.05.020.

Moffat, C., Owens, B., Beardsley, R.C., 2009. On the characteristics of Circumpolar Deep Water intrusions to the west Antarctic Peninsula Continental Shelf. J. Geophys. Res. 114, C05017. http://dx.doi.org/10.1029/2008JC004955.

Montes-Hugo, M., Doney, S.C., Ducklow, H.W., Fraser, W., Martinson, D., Stammerjohn, S.E., Schofield, O., 2009. Recent changes in phytoplankton communities associated with rapid regional climate change along the Western Antarctic Peninsula. Science 323 (5920), 1470–1473. http://dx.doi.org/10.1126/science.1164533.

Morris, E.M., Vaughan, D.G., 2003. Spatial and temporal variation of surface temperature on the Antarctic Peninsula and the limit of viability of ice shelves. In: Domack, E., Leventer, A., Burnett, A., Bindschadler, R., Convey, P., Kirby, M. (Eds.), Antarctic Peninsula Climate Variability: Historical and Paleoenvironmental Perspectives 79. American Geophys. Union, Antarctic Res. Series, Washington, DC, pp. 61–68. http://dx.doi.org/10.1029/079ARS05.

Nicholls, K.W., Østerhus, B., Makinson, K., Gammelsrod, T., Fahrbach, E., 2009. Ice-ocean processes over the continental shelf of the southern Weddell Sea, Antarctica. A review. Rev. Geophys. 47, RG3003. http://dx.doi.org/10.1029/2007/RG000250.

Niiler, P.P., Amos, A., Hu, J.-H., 1991. Water masses and 200 m relative geostrophic circulation in the western Bransfield Strait region. Deep-Sea Res. Part A 38, 943–959. http://dx.doi.org/10.1016/0198-0149(91)90091-S.

Orsi, A.H., Whitworth, T., Nowlin Jr., W.D., 1995. On the meridional extent and fronts of the Antarctic Circumpolar Current. Deep-Sea Res. 42, 641–673.

Poole, R., Tomczak, M., 1999. Optimum multiparameter analysis of the water mass structure in the Atlantic Ocean thermocline. Deep-Sea Res. I 46, 1895–1921.

Prézelin, B.B., Hofmann, E.E., Mengelt, C., Klinck, J.M., 2000. The linkage between Upper Circumpolar Deep Water (UCDW) and phytoplankton assemblages on the west Antarctic Peninsula continental shelf. J. Mar. Res. 58, 165–202. http://dx.doi.org/10.1357/002224000321511133.

Prézelin, B.B., Hofmann, E.E., Moline, M., Klinck, J.M., 2004. Physical forcing of phytoplankton community structure and primary production in continental shelf waters of the Western Antarctic Peninsula. J. Mar. Res. 62, 419–460.

Pritchard, H.D., Ligtenberg, S.R.M., Fricker, H., Vaughan, D.G., van den Broeke, M.R., Padman, L., 2012. Antarctic ice-sheet loss driven by basal melting of ice shelves. Nature 484 (7395), 502–505. http://dx.doi.org/10.1038/nature10968.

Renner, A.H.H., Thorpe, S.E., Heywood, K.J., Murphy, E.J., Watkins, J.L., Meredith, M.P., 2012. Advective pathways near the tip of the Antarctic Peninsula: trends, variability and ecosystem implications. Deep-Sea Res. I. 63, 91–101. http://dx.doi.org/10.1016/j.dsr.2012.01.009.

Rignot, E., Jacobs, S., Mouginot, J., Scheuchl, B., 2013. Ice-shelf melting around Antarctica. Science 341, 266–270. http://dx.doi.org/10.1126/science.1235798.

Robertson, R., Visbeck, M., Gordon, A.L., Fahrbach, E., 2002. Long-term temperature trends in the deep waters of the Weddell Sea. Deep-Sea Res. II 49, 4791–4806. http://dx.doi.org/10.1016/S0967-0645(02)00159-5.

Sangrà, P., Gordo, C., Hernández-Arencibia, M., Marrero-Díaz, A., Rodríguez-Santana, A., Stegner, A., Martínez-Marrero, A., Pelegrí, J.L., Pichon, T., 2011. Bransfield Curr. Syst. Deep-Sea Res. I 58, 390–402. http://dx.doi.org/10.1016/j.dsr.2011.01.011.

Sangrà, P., Stegner, A., Hernández-Arencibia, M., Marrero-Díaz, A., Salinas, C., Aguiar-González, B., Henríquez-Pastene, C., 2017. The Bransfield gravity current. Deep-Sea Res. I 119, 1–15.

Schmidtko, S., Heywood, K.J., Thompson, A.F., Aoki, S., 2014. Multidecadal warming of Antarctic waters. Science 346, 1227–1231. http://dx.doi.org/10.1126/science.1256117.

Sievers, H.A., Nowlin Jr., W.D., 1984. The stratification and water masses at Drake Passage. J. Geophys. Res. 89, 10489–10514.

Smith, D.A., Klinck, J.M., 2002. Water properties on the west Antarctic Peninsula Continental Shelf: a model study of effects of surface fluxes and sea ice. Deep-Sea Res. Ii. 49, 4863–4886.

Smith, C.A., Sardeshmuk, P., 2000. The effect of ENSO on the intraseasonal variance of surface temperature in winter. Int. J. Climatol. 20, 1543–1557.

Smith, R.C., Stammerjohn, S.E., 2001. Variations of surface air temperature and sea ice extent in the western Antarctic Peninsula region. In: Ross, R.M., Hoffmnan, E.E., Quentin, L.B. (Eds.), Foundations for Ecological Research. West of the Antarctic Peninsula (Antarctic Research Series) 70. American Geophysics Union, Washington, DC, pp. 105–121.

Spiridinov, V.A., 1996. A scenario of the Late Pleistocene-Holocene changes in the distributional range of Antarctic krill (*Euphausia superba*). Mar. Ecol. 17, 519–541.

Stammerjohn, S.E., Martinson, D.G., Smith, R.C., Yuan, X., 2008. Trends in Antarctic annual sea ice retreat and advance and their relation to El Niño-Southern Oscillation and Southern Annular Mode. J. Geophys. Res. 113, C03S90. http://dx.doi.org/10.1029/2007JC004269.

Thompson, D.W.J., Wallace, J.M., 2000. Annular modes in the extratropical circulation. Part I: month-to-month variability. J. Clim. 13, 1000–1016.

Timmerman, R., Hellmer, H.H., Beckmann, A., 2002. Simulations of ice-ocean dynamics in the Weddell Sea Part II: interannual variability 1985–1993. J. Geophys. Res. 107 (doi:101029/2000JC00742).

Tokarczyk, R., 1987. Classification of water masses in the Bransfield Strait and Southern part of the Drake Passage using a method of statistical multidimensional analysis. Pol. Polar Res. 8, 333–336.

Tomczak, M., 1981. A multi-parameter extension of temperature/salinity diagram techniques for the analysis of non-isopycnal mixing. Prog. Oceanogr. 10, 147–171.

Tomczak, M., Large, D.G.B., 1989. Optimum multiparameter analysis of mixing in the thermocline of the eastern Indian Ocean (141-16,149). J. Geophys. Res. 94 (C11), 16. http://dx.doi.org/10.1029/JC094iC11p16141.

Turner, et al., 2015. Absence of 21st century warming on Antarctic Peninsula consistent with natural variability. Nature 535, 411–415. http://dx.doi.org/10.1038/nature18645.

Uotila, P., Lynch, A.H., Cassano, J.J., Cullather, R.I., 2007. Changes in Antarctic net precipitation in the 21st century based on Intergovernmental Panel on Climate Change (IPCC) model scenarios. J. Geophys. Res. 112. http://dx.doi.org/10.1029/2006JD007482.

Vaughan, D.G., Marshall, G.J., Connelley, W.M., Parkinson, C., Mulvaney, R., Hodgson, D.A., King, J.C., Pudsey, C.J., Turner, J., 2003. Recent rapid regional climate warming on the Antarctic Peninsula. Clim. Change 60, 243–274.

Van Caspel, M., Schröeder, M., Huhn, O., Hellmer, H.H., 2015. Precursors of Antarctic bottom water formed on the continental shelf off Larsen ice shelf. Deep-Sea Res. I 99, 1–9. http://dx.doi.org/10.1016/j.dsr.2015.01.004.

Van Caspel, M., Hellmer, H.H., Mata, M.M., 2017. On the ventilation of Bransfield Strait deep basins. Deep-Sea Res. II. http://dx.doi.org/10.1016/j.dsr2.2017.09.006.

Van Wijk, E.M., Rintoul, S.R., 2014. Freshening drives contraction of Antarctic Bottom Water in the Australian Antarctic Basin. Geophys. Res. Lett. 41, 1657–1664. http://dx.doi.org/10.1002/2013GL058921.

Von Gyldenfeldt, A.-B., Fahrbach, E., García, M.A., Shröder, M., 2002. Flow variability at the tip of the Antarctic Peninsula. Deep-Sea Res. II 49, 4743–4766.

Whitworth III, T., Nowlin Jr., W.D., Orsi, A.H., Locarnini, R.A., Smith, S.G., 1994. Weddell Sea shelf water in the Bransfield Strait and Weddell-Scotia Confluence. Deep-Sea Res. I 41, 629–641.

Whitworth III, T., Orsi, A.H., Kim, S.J., Nowlin Jr., W.D., Locarnini, R.A., 1998. Water masses and mixing near the Antarctic slope front. In: Jacobs, S.S., Weiss, R.F. (Eds.), Ocean, Ice, and Atmosphere: Interactions at the Antarctic Continental Margin, Antarctic Research Series 75. AGU, Washington, D. C, pp. 1–27 (doi:2007GL030340/AR075p0001).

Wilson, C., Klinkhammer, G.P., Chin, C.S., 1999. Hydrography within the Central and East Basins of the Bransfield Strait, Antarctica. J. Phys. Oceanogr. 465–479.

Yuan, X., 2004. ENSO-related impacts on Antarctic sea ice: a synthesis of phenomenon and mechanisms. Antar. Sci. 16, 415–425.

Youngs, M.K., Thompson, A.F., Flexas, M.M., Heywood, K.J., 2015. Weddell Sea export pathways from surface drifters. J. Phys. Oceanogr. 45, 1068–1085. http://dx.doi.org/10.1175/JPO-D-14-0103.1.

Zhou, M., Niiler, P.P., Hu, J.-H., 2002. Surface currents in the Bransfield and Gerlache Straits, Antarctica. Deep-Sea Res. I 49 (2), 267–280. http://dx.doi.org/10.1016/S0967-0637(01)00062-0.

Zhou, M., Niiler, P.P., Zhu, Y., Dorly, R.D., 2006. The western boundary current in the Bransfield Strait, Antarctica. Deep-Sea Res. I 53, 1244–1252. http://dx.doi.org/10.1016/j.dsr.2006.04.003.